European Journal of Medicinal Chemistry 219 (2021) 113424

Contents lists available at ScienceDirect

European Journal of Medicinal Chemistry

journal homepage: http://www.elsevier.com/locate/ejmech

Identification and optimization of 3-bromo-*N*'-(4-hydroxybenzylidene)-4-methylbenzohydrazide derivatives as mTOR inhibitors that induce autophagic cell death and apoptosis in triple-negative breast cancer

Tian Xu [a, 1], Jifa Zhang [a, 1], Chengcan Yang [a], Ryszard Pluta [c], Guan Wang [a, **], Tinghong Ye [a, ***], Liang Ouyang [a, b, *]

[a] State Key Laboratory of Biotherapy and Cancer Center, Sichuan University-Oxford University Huaxi Gastrointestinal Cancer Centre, National Clinical Research Center for Geriatrics, West China Hospital, Sichuan University, Chengdu, 610041, China
[b] State Key Laboratory of Esophageal Cancer Prevention and Treatment, Zhengzhou University, Zhengzhou, 450001, China
[c] Laboratory of Ischemic and Neurodegenerative Brain Research, Mossakowski Medical Research Institute, Polish Academy of Sciences, Warsaw, Poland

ARTICLE INFO

Article history:
Received 27 January 2021
Received in revised form
17 March 2021
Accepted 28 March 2021
Available online 3 April 2021

Keywords:
TNBC
mTOR
Pharmacophore-based virtual screening
Autophagy
mTOR inhibitors

ABSTRACT

Triple negative breast cancer (TNBC) has a worse prognosis than other types of breast cancer due to its special biological behavior and clinicopathological characteristics. TNBC cell proliferation and progression to metastasis can be suppressed by inducing cytostatic autophagy. mTOR is closely related to autophagy and is involved in protein synthesis, nutrient metabolism and activating mTOR promotes tumor growth and metastasis. In this paper, we adopted the strategy of structure simplification, aimed to look for novel small-molecule inhibitors of mTOR by pharmacophore-based virtual screening and biological activity determination. We found a lead compound with 3-bromo-N'-(4-hydroxybenzylidene)-4-methylbenzohydrazide for rational drug design and structural modification, then studied its structure-activity relationship. After that, compound **7c** with the best TNBC cells inhibitory activities and superior mTOR enzyme inhibitory activity was obtained. In addition, we found that compound **7c** could induce autophagic cell death and apoptosis in MDA-MB-231 and MDA-MB-468 cell lines. In conclusion, these findings provide new clues for our 3-bromo-N'-(4-hydroxybenzylidene)-4-methylbenzohydrazide derivatives, which are expected to become drug candidates for the treatment of TNBC in the future.

1. Introduction

Breast cancer is a malignant tumor that occurs in the epithelial tissue of the breast [1,2]. Triple-negative breast cancer (TNBC) refers to breast cancer that is negative for estrogen receptor (ER), progesterone receptor (PR) and proto-oncogene Her-2 by immunohistochemical examination of cancer tissue [3–5]. TNBC has a worse prognosis than other types due to its special biological behavior and clinicopathological characteristics [6–8]. Due to the lack of three main hormone-related receptors at the same time, targeted therapy for TNBC remains challenging. Previous studies have shown that enhanced autophagy is associated with drug resistance of TNBC [9,10], and autophagy also leads to apoptosis [11,12]. Moreover, it has been reported that TNBC cell proliferation and progression to metastasis can be suppressed by inducing cytostatic autophagy [13,14]. Therefore, it is of great significance and hope to find novel compounds activating autophagy as therapeutic agents for TNBC [15,16].

mTOR is a serine/threonine kinase and the domain structure of mTOR consists of 6 functional regions [17,18]. mTOR includes two protein complexes with different functions: mTORC1 and mTORC2. Activating mTOR can not only cause a wide range of precancerous effects, including cell cycle progression, cell proliferation and

* Corresponding author. State Key Laboratory of Biotherapy and Cancer Center, Sichuan University-Oxford University Huaxi Gastrointestinal Cancer Centre, National Clinical Research Center for Geriatrics, West China Hospital, Sichuan University, Chengdu, 610041, China.
** Corresponding author.
*** Corresponding author.
E-mail addresses: guan8079@163.com (G. Wang), yeth1309@scu.edu.cn (T. Ye), ouyangliang@scu.edu.cn (L. Ouyang).
[1] These authors contributed equally to this work.

https://doi.org/10.1016/j.ejmech.2021.113424
0223-5234/

survival, but also cause AKT phosphorylation and control the function of cytoskeletal proteins [19–23]. mTOR plays a vital role in regulating autophagy as many signal transduction pathways focus on the target of highly conserved mTOR. The development of mTOR inhibitors that can regulate autophagy is an effective strategy for the treatment of breast cancer. Mutations in upstream inhibitory molecules of mTOR can usually lead to excessive activation of mTOR and at the same time weakened autophagy, which is closely related to the occurrence and development of tumors [24]. In some cases, autophagy can promote cell apoptosis or enhance cell apoptosis, thereby promoting cell death [25]. In addition, the important role of autophagy in cell cycle arrest, aging and response to oxidative stress can also limit the further growth of tumors [26]. Therefore, inhibiting mTOR activity, inducing autophagy, and promoting autophagic death of cells, not only can reduce the pressure of toxic proteins, but also have an anti-tumor effect.

Rapamycin (**1**) is the first mTOR inhibitor to be discovered [27–31]. Rapamycin is a 36-carbon macrocycle, and its research is still limited to semi-synthetic derivatives [32]. Rapamycin and its analogues inhibit the expression of mTORC1 and can interact with insulin receptor substrate 1 (IRS-1) form a negative feedback pathway, causing overactivation of AKT. AKT signaling pathway is frequently dysregulated in up to 70% of human breast cancer, and is associated with overall poor prognosis in cancer [33–36]. Due to the complex structure and potential AKT activation, the application of Rapamycin and its analogues is limited [37]. Finding novel small-molecule inhibitors of mTOR can avoid the limitation of Rapamycin and its analogues and has become one of the focuses of chemists. Hitherto, multiple mTOR small-molecule inhibitors have been reported and some of them have entered clinical researches. As shown in Fig. 1A, compounds **3** (pp242), **4** (NVP-BEZ235), **5** (AZD8055), **6** (MLN0128) and **7** (PI-103) are all small-molecule mTOR inhibitors that have entered clinical research in various types of tumors, including advanced solid tumors, metastatic breast cancer, and metastatic renal cell carcinoma [38–42]. It is worth mentioning that compound **6** has entered phase I study in patients with metastatic Triple-negative breast cancer.

In this paper, we explored the pharmacophore model of mTOR inhibitors by studying their common anchoring properties and the distance between target proteins, and considering favorable interactions of multiple mTOR active molecules and active sites. According to the representative inhibitor-protein complex system, we read the three-dimensional coordinates of inhibitors, analyzed their binding characteristics, and got the key amino acids of small molecules interacting with mTOR. By combining extraction of important amino acid sites, pharmacophore simulation and virtual screening, we designed a series of new skeletons and obtained the lead compound with 3-bromo-N'-(4-hydroxybenzylidene)-4-methylbenzohydrazide. Then, 44 compounds were synthesized through chemical modification based on rational drug design and structure activity relationship analysis. In the follow-up biological evaluation, we found that **7c** showed good inhibitory activities in MDA-MB-231 and MDA-MB-468 cells and mTOR kinase. Further results showed that **7c** could induce autophagy and apoptosis of MDA-MB-231 and MDA-MB-468 cell lines cells by inhibiting mTOR, and it will provide a promising new therapeutic method for the treatment of TNBC.

2. Results

2.1. Virtual screening and chemistry

In order to find new small molecules with mTOR inhibitory activity, we planned to combine pharmacophore simulation screening with analysis of important amino acid sites [43]. Here, we first selected some mTOR small molecule inhibitors to get the inhibitor-mTOR protein complex, and then we can get the overlapping inhibitor protein system by overlapping the complexes (Fig. S1). The next work was divided into two kinds of synchronization. Firstly, based on the interaction mode of inhibitor-mTOR complex and the energy contribution of each residue, we constructed a small molecule pharmacophore model targeting mTOR in discovery studio. Starting from the binding mode of the complexes, we extracted five pharmacophore characteristics of mTOR targeting: mTOR inhibitors contained an aromatic ring, a hydrogen bond donor, a hydrogen bond receptor and two negative charge centers; Then, we extracted key characteristics from the pharmacophore model and analyzed the distance between each key pharmacophore to obtain the small molecule pharmacophore targeting mTOR for subsequent virtual screening. While constructing the pharmacophore model, we read the three-dimensional coordinates of mTOR inhibitor-protein complex. mTOR inhibitors were anchored in mTOR protein. Firstly, each ligand was adjusted to the top 1 position for subsequent analysis. It was important to analyze the amino acid active sites of reported mTOR inhibitors. The binding characteristics of mTOR inhibitors were analyzed subsequently, and the key amino acid inhibitory sites were VAL2240, TRP2239, ILE2237, ILE2356, ASP2195, ARG2348 and MET2345.

Next, virtual screening of small-molecule compounds targeted by mTOR was performed from databases including SPECS, Chemdiv, ACDB and MCDB. According to Lipinski's five drug principles, a preliminary screening of the compound library was carried out, and 98,460 compounds were obtained. Next, we screened the molecules in Discovery Studio based on the pharmacophore targeting mTOR and the ability to bind to amino acid residues. According to the fitting value of the small molecules and the pharmacophore groups and the binding effect with the key amino acid residues, 100 small molecules with the highest fitting values were extracted.

We further selected and synthesized the lead compound **A1** with the best interaction energy and score according to Lipinski's five drug-like principles, Libdock and Cdocker protocol, pharmacophore model and the binding ability with key amino acids. (Fig. 1B). The IC_{50} of **A1** was 10.34 ± 0.23 μM for A549 cells, 9.27 ± 0.14 μM for MDA-MB-231 cells and 8.76 ± 0.31 μM for MDA-MB-468 cells. At the same time, the mTOR IC_{50} of **A1** was 3.96 μM, indicating that **A1** could be used as a lead compound for further structural modification.

In order to optimize the structure of compound **A1**, we first replaced the linker between the two benzene rings, and synthesized a series of derivatives according to the synthetic route outlined in Scheme 1. The synthesis of compounds **1b-14b** was carried out through one-step reactions of different substituted phenyl isocyanates and different amines. Isocyanate and amine were stirred and reacted in acetonitrile at room temperature. The syntheses were monitored by TLC and the reactions were completed within 4–16 h. After the reaction solutions were spin-dried, they were purified to obtain compounds **1b-14b**.

In Scheme 2, using methyl benzoate as starting material, oxalyl chloride as the solvent and reactant, a little DMF as the catalyst, the reactions were refluxed for 8–16 h, then the reaction solutions were spin-dried and purified with DCM: methanol = 10:1 to obtain the intermediate acid chlorides **1d-2d**. Subsequently, under the protection of N_2, the acid chlorides and different amines were stirred and reacted in DMF at room temperature for 8–12 h. After the reactions completed, they were quenched by water and extracted with DCM. The organic phases were concentrated and purified with dichloromethane: methanol = 10:1 to obtain the final compounds **6a-7a, 23a-25a**.

We examined the effect of various substituted groups and

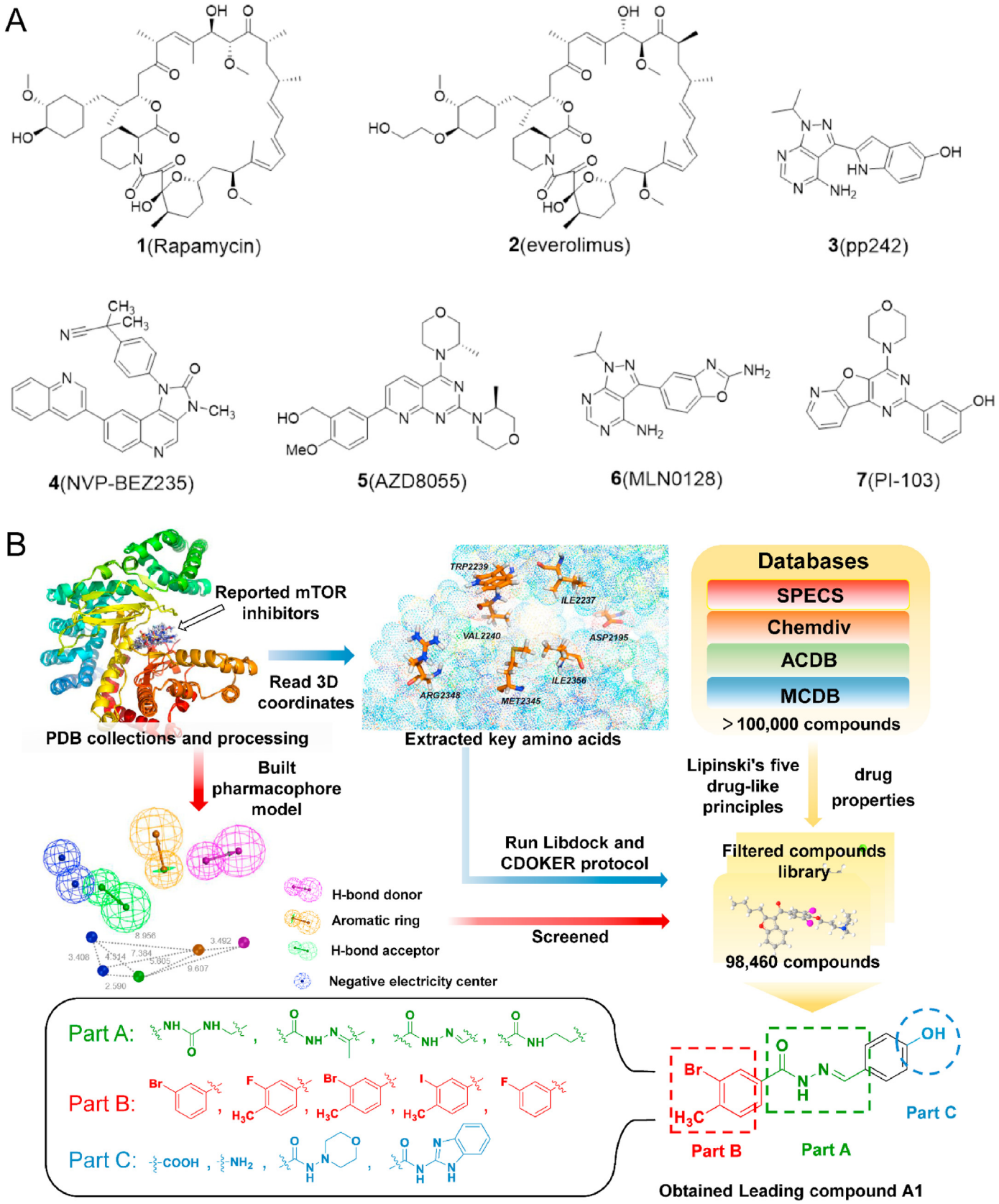

Fig. 1. A. The structures of some reported mTOR inhibitors. **B.** The workflow of designing mTOR inhibitors based on pharmacophore model, extracted amino acid, and virtual screening.

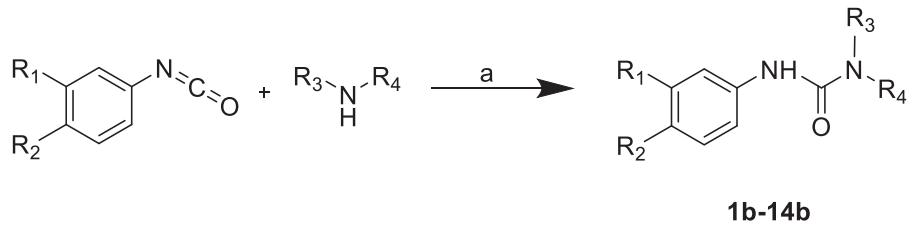

Scheme 1. Reagents and conditions: (a) Acetonitrile, r.t.

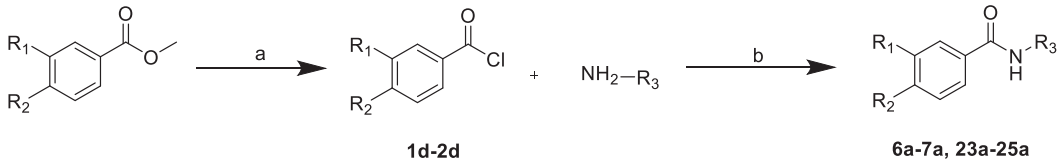

Scheme 2. Reagents and conditions: (a) Oxalyl chloride, DMF, reflux; (b) N_2, Pyridine, overnight, r.t.

synthesized a series of derivatives according to the synthetic routes outlined in Scheme 3. First, the reaction of methyl benzoate and 80% hydrazine hydrate yielded intermediates **1e-6e**. Then, obtained intermediates and different amines refluxed for 8−24 h in methanol, using a few drops of glacial acetic acid as the catalyst. Monitored by TLC, the reactions were taken off and spin-dried, and purified using dichloromethane: methanol = 10:1. And then we can obtain compounds **1a-2a, 4a-5a, 8a-9a, 11a, 13a-16a, 19a-22a, 3c, 5c, 9c**.

In Scheme 4, using a little DMF as the catalyst, **19a-20a** acted with oxalyl chlorides and refluxed for 8 h−16 h, then the solutions were spin-dried and purified with DCM: methanol = 10:1 to obtain the intermediates **1f-4f**. Subsequently, under the protection of N_2, the acid chlorides and different amines were stirred and reacted in DMF at room temperature for 8−12 h. The reactions were quenched by water and extracted with DCM when reactions completed. The organic phases were concentrated and then purified with dichloromethane: methanol = 10:1, and then we obtained the final compounds **1c-2c, 6c-8c, 10c**.

2.2. SAR relationship of the synthesized compounds

Compared with **A1**, most of the urea compounds (**1b-14b**) had significantly reduced mTOR inhibition and inhibitory effects on breast cancer cells and lung cancer cells (Table 1). At the same time, the mTOR IC_{50} and MDC positive ratio of these compounds were not as good as positive controls, Rapamycin and Temsirolimus. Rapamycin and Temsirolimus were both mTOR inhibitors with the ability of autophagy induction [44,45]. The autofluorescent agent MDC was recently introduced as a specific autophagolysosome marker to analyze the autophagic process [46,47]. The previous work of our research group also proved that MDC staining can effectively detect the level of autophagy in cells [48]. Some of the compounds (**10b, 12b-14b**) had less inhibitory effects compared with other compounds of the same kind, which may attribute to the substitutions of fluorine or trifluoromethyl on the benzene rings that affected the effectiveness of the molecules. Further research found that when the double bond was eliminated, compound **6a** could not achieve better cancer cell inhibition rates, even leading to mTOR inhibition cliff down. A methyl group was introduced at the C-terminus of the double bond, and the test results showed that the compound's inhibitory effect on cancer cells and mTOR increased significantly after the introduction of the methyl group. In addition, the test result of **7a** showed that shorting the length of compound cannot significantly increase the inhibition rates of breast cancer cells or mTOR (Table 2). After chain discussion, the lead compound **1a** was obtained, with the IC_{50} of 6.71 ± 2.23 μM, 8.46 ± 1.19 μM, 10.07 ± 1.64 μM for MDA-MB-231, MDA-MB-468 and A549 cells, respectively and an IC_{50} of 2.01 μM for mTOR. (Table 3).

Our lead compound **1a** was linear in shape, and the pharmacophore consisted of two benzene rings and an amidonitro-carbon double bond linker. Previous studies have shown that this linker is an important core structure maintaining cells inhibitory activities. Therefore, in the later molecule design, this part of the structure was retained, and the substituents on the benzene ring were mainly modified. Under this circumstance, we further conducted a structure-activity study on the benzene ring and groups of the compound to obtain better cytostatic activity. The results show that the different substituents of the R_1, R_2 and R_3 groups on the benzene rings have different effects on the inhibitory activities of mTOR and TNBC cells. When R_1 is substituted by bromine, R_2 is substituted by hydrogen, and R_3 is 4-benzoic acid, compound **19a** showed the best inhibitory activities on mTOR and MDA-MB-231 and MDA-MB-468 cells than other compounds (Table 3).

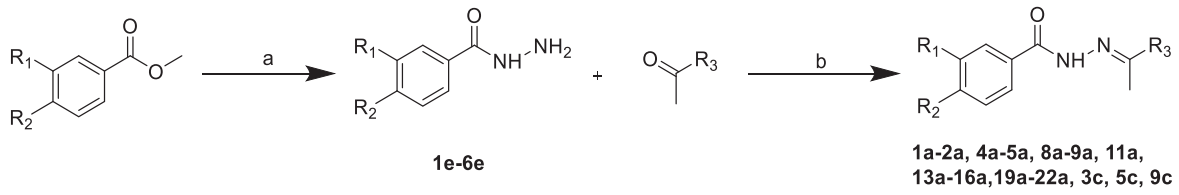

Scheme 3. Reagents and conditions: (a) Hydrazine hydrate, heat; (b) Methanol, acetic acid, reflux.

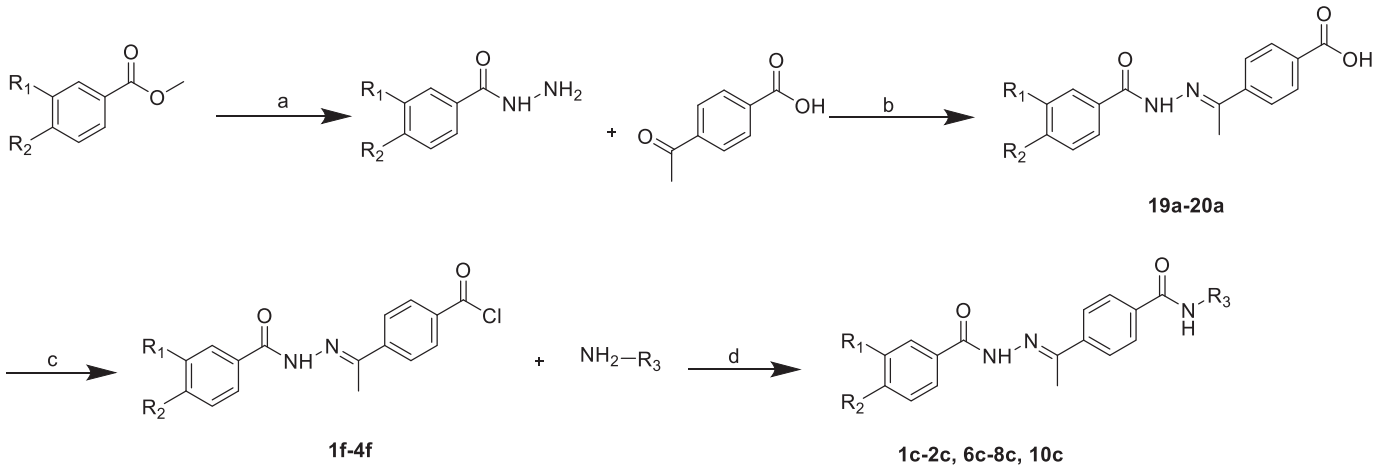

Scheme 4. Reagents and conditions: (a) Hydrazine hydrate, heat; (b) Methanol, acetic acid, reflux; (c) Oxalyl chloride, DMF, reflux; (d) N_2, Pyridine, overnight.

Moreover, **19a** also showed better MDC positive ratio than other compounds.

To further optimize the structure of the lead compound **19a**, we realized that extending the tail group of the molecule will be a feasible method, because there are large hydrophobic pockets in the surface area of mTOR. By extending the tail group, more interactions such as hydrophobic interaction , π−π stacking interaction and hydrogen bonding can be formed. We analyzed the different parts contained in the reported effective mTOR inhibitors and selected them as modifiable tail groups. For example, the molecular end of pp242 has a benzopyrrole structure, which can maintain the hydrophobic effect with the binding pocket of mTOR. Therefore, we introduced a group of similar structures as the terminal substituents attached to the benzene ring to carry out the third round of structural optimization. We speculated that these structures should be able to form various interactions with the pockets of mTOR. Therefore, we synthesized the target compounds **1c-2c, 6c-8c, 10c** and detected their inhibition rates in TNBC cells and mTOR. The results showed that the inhibitory rates of this series of compounds on TNBC cells and mTOR were significantly improved (Table 4). The results showed that when the tail group was benzimidazole, the inhibitory rate of compound **7c** on mTOR can reach 79.8%, and the IC_{50} is 0.304 μM. However, when the groups were substituted with indole and other groups, the observed mTOR IC_{50} values were not as good as that of compound **7c**. Meanwhile, compared with the positive controls Rapamycin and Temsirolimus, compound **7c** had better inhibitory activity on TNBC cells, and the MDC positive ratio of **7c** in MDA-MB-231 cells was higher than that of Temsirolimus, indicating that **7c** might have stronger autophagy induction in TNBC cells.

The SAR was summarized as follows: (1) The amido-nitrogen-carbon double bond linker of the series of target compounds acted as an important pharmacophore for cells inhibitory activities and mTOR inhibitory activity, ensuring effective TNBC cells proliferation inhibition and mTOR inhibition. (2) As an effective active group, the imidazole group helped to inhibit the activity of mTOR. (3) The C—C double bond on the connecting chain was very important. When the double bond was cancelled, the inhibition of the target compounds on mTOR and TNBC cells were reduced. Shortening the length of the alkyl chain would also affect the efficacy. (4) The different substituents on the two benzene rings had different effects on the inhibition of mTOR and MDA-MB-231 and MDA-MB-468 cells, and the compound with R_1 substituted by bromine and R_2 substituted by hydrogen showed the best efficacy. The inhibitory activities of compounds with other substituents decreased significantly. Compound 7c showed better MDC positive ratio than the positive control Temsirolimus, indicating that 7c could induce autophagy in MDA-MB-231 cells.

2.3. Identification of 7c as a new mTOR inhibitor

Molecular docking showed that compound **7c** had more interactions with mTOR than **A1**, which may be the reason why the inhibition rates of **7c** were better than those of **A1** (Fig. 2A, Fig. S2).Based on the excellent cytostatic activities of **7c**, we tested the mTOR kinase inhibitory activity of **7c**, and the results showed that the mTOR IC_{50} of **7c** was 0.304 μM (Fig. 2B).In addition, in order to confirm whether **7c** can inhibit the kinase activity of mTOR in cells, we tested the levels of mTOR and mTOR downstream substrates such as AKT, 4EBP1 and P70S6K and phosphorylated substrate levels in MDA-MB-231 and MDA-MB468 cells. The results showed that the levels of p-mTOR (Ser2448) was reduced (Fig. 2C). Besides, the levels of AKT, 4EBP1 and P70S6 in MDA-MB-231 and MDA-MB468 cells were reduced, and the levels of p-AKT (Ser473), p-4EBP1 (Thr37/46) and p-P70S6K (Thr389) were reduced more. This indicated that **7c** can inhibit the activity of mTOR in triple-negative breast cancer cells (Fig. 2D).

2.4. 7c inhibits colony formation and promotes cell apoptosis in MDA-MB-231 and MDA-MB-468 cells

Hoechst 33258 staining was used to observe the changes of the two kinds of cells treated with different concentrations of **7c**. It was observed that cell numbers decreased significantly in a dose-dependent manner (Fig. 3A). **7c** also significantly inhibited the growths and clone formations of MDA-MB-231 and MDA-MB-468 cells in a concentration dependent manner (Fig. 3B). Moreover, flow cytometry showed that compound **7c** could induce apoptosis in two triple negative breast cancer cells, and we believed that the apoptosis may be caused by changes in endogenous pathways (Fig. 3C). Based on the results of Flow Cytometry, we detected the expression of apoptosis related proteins by Western blot. As shown, **7c** treatment resulted in decreases in Bcl-2, increases in the conversion of Bax, and increases in Cleaved-caspase3 levels in MDA-MB-231 and MDA-MB-468 cells (Fig. 3D). In conclusion, the results showed that **7c** could significantly induce apoptosis in MDA-MB-231 and MDA-MB-468 cells.

Table 1
SAR study on the linker.

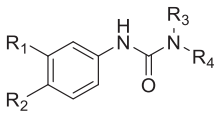

Compound	R_1	R_2	R_3	R_4	IC_{50} (μM)[a,b]			mTOR IC_{50} (μM)	MDC positive ratio %(1 μM)[c]
					A549	MDA-MB-231	MDA-MB-468		
1b	H	CF_3	H	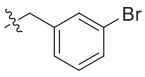	26.43 ± 1.15	20.76 ± 0.12	24.32 ± 0.29	15.82	9.10 ± 1.28
2b	H	CF_3	CH_3	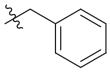	28.75 ± 1.07	21.19 ± 0.55	21.94 ± 0.47	10.13	7.34 ± 0.93
3b	H	CF_3	H	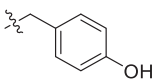	36.72 ± 0.32	22.94 ± 0.18	17.50 ± 0.48	10.29	8.29 ± 1.01
4b	Cl	H	H	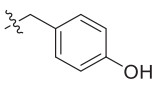	31.20 ± 0.37	19.54 ± 2.43	25.95 ± 1.41	27.06	9.22 ± 0.86
5b	F	H	H	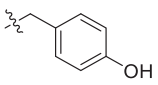	22.30 ± 2.23	27.72 ± 1.29	34.06 ± 0.57	> 30	8.31 ± 5.37
6b	Cl	H	H	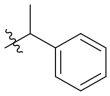	24.83 ± 1.24	22.60 ± 0.72	23.71 ± 0.86	> 30	9.25 ± 3.04
7b	F	H	H	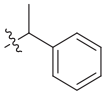	33.05 ± 0.32	34.06 ± 1.24	31.94 ± 0.99	16.88	8.29 ± 1.66
8b	H	CH_3	H	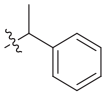	31.20 ± 2.14	31.69 ± 0.69	27.50 ± 1.29	15.80	9.01 ± 2.60
9b	H	CH_3	H	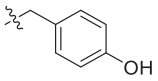	21.20 ± 2.31	15.19 ± 1.14	25.95 ± 1.17	11.65	10.02 ± 0.81
10b	F	H	H	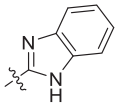	19.76 ± 2.59	19.00 ± 2.77	24.06 ± 2.80	4.93	8.32 ± 3.92
11b	H	CF_3	H	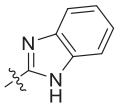	23.50 ± 1.02	22.82 ± 0.96	23.71 ± 1.58	23.68	8.20 ± 1.30
12b	F	H	H	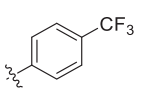	11.52 ± 1.15	10.28 ± 2.03	11.94 ± 2.21	12.56	7.22 ± 2.59
13b	F	H	H	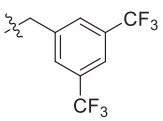	12.54 ± 1.72	13.82 ± 2.85	17.50 ± 1.09	17.63	8.77 ± 1.04

Table 1 (*continued*)

Compound	R_1	R_2	R_3	R_4	IC_{50} (μM)[a,b]			mTOR IC_{50} (μM)	MDC positive ratio %(1 μM)[c]
					A549	MDA-MB-231	MDA-MB-468		
14b	H	CF_3	H	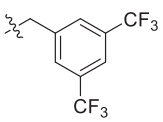	13.34 ± 0.78	16.87 ± 0.94	17.95 ± 1.17	20.43	9.62 ± 0.91
Rapamycin					30.72 ± 1.91	35.79 ± 1.38	37.20 ± 0.77	0.0008	31.03 ± 1.54
Temsirolimus					11.81 ± 2.46	17.57 ± 1.35	10.89 ± 1.73	2.29	15.33 ± 2.80

[a] Each compound was tested in triplicate; the data are presented as the mean ± SEM (n = 3).
[b] IC_{50} values obtained with cell viability assay for 24 h.
[c] Determined by flow cytometry analysis using MDC staining; the data are presented as the mean ± SEM (n = 3).

Table 2
SAR study on the linker.

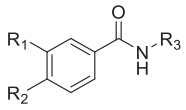

Compound	R_1	R_2	R_3	IC_{50} (μM)[a,b]			mTOR IC_{50} (μM)	MDC positive ratio %(1 μM)[c]
				A549	MDA-MB-231	MDA-MB-468		
6a	Br	CH_3	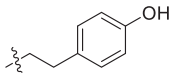	33.98 ± 1.22	41.71 ± 0.57	33.71 ± 0.83	> 30	11.23 ± 0.40
7a	Br	CH_3	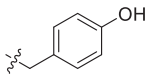	33.83 ± 1.47	33.37 ± 0.99	41.94 ± 1.72	> 30	12.73 ± 0.91
23a	Br	CH_3	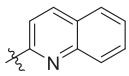	31.57 ± 1.16	37.95 ± 0.67	27.50 ± 0.80	17.86	13.81 ± 1.96
24a	Br	CH_3	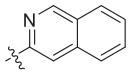	26.37 ± 1.58	32.12 ± 0.35	25.95 ± 0.76	15.27	11.80 ± 1.53
25a	H	OCF_3	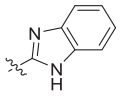	27.53 ± 2.11	29.03 ± 1.53	24.06 ± 2.06	3.99	11.22 ± 2.74
Rapamycin				30.72 ± 1.91	35.79 ± 1.38	37.20 ± 0.77	0.0008	31.03 ± 1.54
Temsirolimus				11.81 ± 2.46	17.57 ± 1.35	10.89 ± 1.73	2.29	15.33 ± 2.80

[a] Each compound was tested in triplicate; the data are presented as the mean ± SEM (n = 3).
[b] IC_{50} values obtained with cell viability assay for 24 h.
[c] Determined by flow cytometry analysis using MDC staining; the data are presented as the mean ± SEM (n = 3).

2.5. 7c induces autophagy via mTOR inhibition

mTOR is closely related to autophagy. Studies have shown that inhibition of mTOR can effectively induce autophagy. Our previous results have shown that **7c** can inhibit cell viability, so we next examined the ability of **7c** to induce autophagy in MDA-MB-231 and MDA-MB-468 cells. First of all, we observed that **7c** could induce the autophagy flux of MDA-MB-231 and MDA-MB-468 cells by GFP-mRFP-LC3 under inverted microscope (Fig. 4A). In order to further evaluate autophagy, we detected the expression of autophagy related proteins by Western blot. As expected, **7c** treatment resulted in significant increases in autophagy, such as decreases in autophagy substrate p62, increases in the conversions of LC3I to LC3II, and increases in Beclin1 levels. In conclusion, the results showed that **7c** could significantly induce autophagy in MDA-MB-231 and MDA-MB-468 cells (Fig. 4B). These results suggested that **7c** could induce autophagy via mTOR inhibition.

2.6. 7c induces autophagic cell death in TNBC cells

Based on the current experimental data, we want to further explore the relationship between **7c** induced autophagy and TNBC cell growth inhibition. Autophagy inhibitor 3-methyladenine (3-MA) can inhibit autophagy by interrupting the formation of autophagosome, which is often used to block the induction of autophagy [49]. Based on previous work, 3-MA was used to prove the relationship between cell death and autophagy [50]. Therefore, we used 3-MA to carry out follow-up verification in our study. We found that the survival rate of cells treated with **7c** and 3-MA was significantly lower than that of cells treated with 3-MA alone

Table 3
SAR study on two benzene rings.

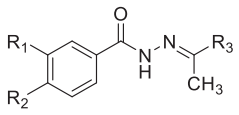

Compound	R_1	R_2	R_3	IC_{50} (μM)[a,b]			mTOR IC_{50} (μM)	MDC positive ratio %(1 μM)[c]
				A549	MDA-MB-231	MDA-MB-468		
1a	Br	CH_3	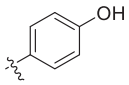	10.07 ± 1.64	6.71 ± 2.23	8.46 ± 1.19	2.01	19.27 ± 2.48
2a	Br	CH_3	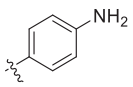	13.57 ± 2.04	9.91 ± 1.87	12.12 ± 1.74	7.30	18.90 ± 2.62
4a	Br	H	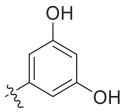	10.29 ± 1.09	9.13 ± 0.94	10.97 ± 1.18	8.20	16.33 ± 0.57
5a	Br	H	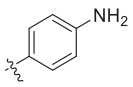	13.04 ± 2.13	10.86 ± 1.27	13.07 ± 3.17	6.21	15.81 ± 1.49
8a	Br	CH_3	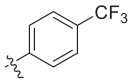	9.07 ± 1.77	9.30 ± 1.24	9.91 ± 1.80	4.76	18.65 ± 2.84
9a	Br	CH_3		12.44 ± 0.96	10.96 ± 1.45	8.69 ± 1.91	5.24	15.26 ± 2.17
11a	I	CH_3	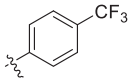	9.46 ± 2.78	8.30 ± 3.12	8.76 ± 1.18	1.98	14.89 ± 2.29
13a	F	H	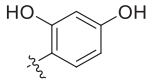	15.41 ± 3.14	10.75 ± 1.62	9.24 ± 2.04	4.22	15.04 ± 1.68
14a	I	CH_3	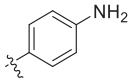	9.93 ± 2.79	8.46 ± 2.14	9.54 ± 1.87	5.08	14.28 ± 3.17
15a	I	H	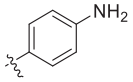	13.04 ± 3.05	13.05 ± 2.44	8.30 ± 1.67	4.79	15.27 ± 1.83
16a	F	CH_3	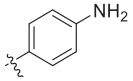	11.95 ± 1.04	8.40 ± 1.80	9.55 ± 2.53	4.32	15.44 ± 1.37
19a	Br	H	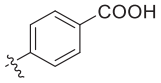	7.78 ± 2.79	7.50 ± 1.83	5.51 ± 0.97	0.69	19.83 ± 1.65
20a	I	H	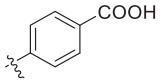	8.91 ± 2.16	8.96 ± 1.83	6.37 ± 1.45	0.82	17.20 ± 2.43
21a	I	CH_3		11.27 ± 1.10	9.08 ± 2.56	10.35 ± 2.40	1.66	16.25 ± 1.64

Table 3 (*continued*)

Compound	R_1	R_2	R_3	IC_{50} (μM)[a,b]			mTOR IC_{50} (μM)	MDC positive ratio %(1 μM)[c]
				A549	MDA-MB-231	MDA-MB-468		
22a	I	H		9.84 ± 1.48	12.53 ± 1.90	12.05 ± 1.78	1.17	15.79 ± 2.61
3c	Br	H		12.57 ± 1.88	14.78 ± 2.06	14.79 ± 2.70	0.95	15.32 ± 0.84
5c	I	CH_3		11.12 ± 1.07	10.12 ± 1.89	10.12 ± 1.68	1.02	14.81 ± 0.41
9c	F	H		14.24 ± 2.78	9.24 ± 1.64	9.76 ± 1.99	43.60	14.36 ± 1.57
Rapamycin				30.72 ± 1.91	35.79 ± 1.38	37.20 ± 0.77	0.0008	31.03 ± 1.54
Temsirolimus				11.81 ± 2.46	17.57 ± 1.35	10.89 ± 1.73	2.29	15.33 ± 2.80

[a] Each compound was tested in triplicate; the data are presented as the mean ± SEM (n = 3).
[b] IC_{50} values obtained with cell viability assay for 24 h.
[c] Determined by flow cytometry analysis using MDC staining; the data are presented as the mean ± SEM (n = 3).

(Fig. 5A). Clone formation assay also confirmed this result (Fig. 5B), indicating that the inhibition of **7c** on TNBC cell growth is autophagy dependent. Subsequently, we performed flow cytometry analysis to examine the apoptosis rate of TNBC cells co-treated with **7c** and 3-MA (Fig. 5C). The results showed that 3-MA could partially reverse the apoptosis induced by **7c**. In conclusion, these data suggest that **7c** could induce autophagic cell death in TNBC cells.

In conclusion, these data suggest that the death of TNBC cells induced by **7c** is autophagy dependent. Although autophagy and apoptosis have significant differences in metabolic pathways and morphology, their signaling pathways are inextricably linked. Based on our experimental results, autophagy inhibitor 3-methyl adenine (3-MA) can reduce cell apoptosis induced by **7c**. In this case, autophagy and apoptosis cooperate to induce cell death. It has also been proved that the antibacterial drug chloroiodoquinoline can induce autophagic death and apoptosis of leukemia cells and myeloma cells by disrupting mTOR signaling pathway [51]. We speculated that **7c** could induce autophagic death and apoptosis of TNBC cells via mTOR inhibition.

3. Conclusions

Triple negative breast cancer (TNBC) has a worse prognosis than other types of breast cancer due to its special biological behavior and clinicopathological characteristics. Autophagy is associated with drug resistance of TNBC, and inducing autophagy could suppress TNBC cell proliferation and progression to metastasis. mTOR plays a vital role in regulating autophagy as many signal transduction pathways focus on the target of highly conserved mTOR. The development of mTOR inhibitors that can regulate autophagy is an effective strategy for the treatment of breast cancer. However, the application of mTOR inhibitor Rapamycin and its analogues is limited due to the complex structure and potential AKT activation. Finding novel small-molecule inhibitors of mTOR can avoid the limitation of Rapamycin and has become one of the focuses of chemists.

To conclude, we have developed a new mTOR pathway inhibitor based on the strategy of structure simplification through the integrated use of multilayer virtual screening and biological determination. Based on the strategy of simplification, we explored the pharmacophore model and read the three-dimensional coordinates of the key amino acids, and then we selected and synthesized compound **A1** with the best interaction energy and score according to Lipinski's five drug-like principles, Libdock and Cdocker protocol. Subsequently, the structure optimization of the compound and the study of the mechanism of the optimal compound are carried out. The results showed that compound **7c** exhibited significant inhibitory activity on mTOR with an IC_{50} of 0.304 μM. The protein levels of p-AKT (Ser473), p-4EBP1 (Thr37/46) and p-P70S6K (Thr389) were significantly decreased treated with **7c**. At the same time, compound **7c** could inhibit the formation of MDA-MB-231 and MDA-MB-468 cell clones and induce apoptosis in a concentration-dependent manner. In addition, we further proved that compound **7c** could induce autophagic cell death in MDA-MB-231 and MDA-MB-468 cells. These findings bring new highlights to compound **7c**, which could be further used as a promising drug candidate for the treatment of TNBC in the future.

4. Experimental section

4.1. Cell culture, reagents and antibodies

All cell lines used in this study were purchased from the American Type Culture Collection (ATCC, Manassas, Virginia, USA). A549 and MDA-MB-231 cells were cultured in Dulbecco's modified Eagle medium (DMEM) supplemented with 10% fetal bovine serum and incubated with 5% CO_2 at 37 °C. MDA-MB-468 cells were cultured in RPMI 1640 medium supplemented with 10% fetal bovine serum, and incubated with 5% CO_2 at 37 °C. MTT (#M2128), Rapamycin and Temsirolimus were purchased from Sigma-Aldrich (St. Louis, Missouri, USA). p-AKT (#4060S), P70S6K (#2708S), p-P70S6K (#9206S), 4EBP1 (#9644), p-4EBP1 (#2855), p62 (#8025), Bax (#5023), Bcl-2 (#2870), Caspase-3 (#9662) purchased from Cell Signaling Technologies (USA Boston, Massachusetts), LC3B (ab51520), Beclin1 (ab207612), mTOR (ab134903), p-mTOR (ab109268) were purchased from abcam, GAPDH (60004-1-Ig), anti-AKT (#10176-2-AP) was purchased from Proteintech. GFP/mRFP-LC3 (HB-AP2100001) was purchased from HANBIO (China).

Table 4
SAR study on terminal groups.

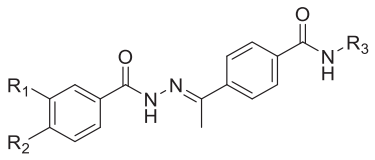

Compound	R_1	R_2	R_3	IC_{50} (μM)[a,b]			mTOR IC_{50} (μM)	MDC positive ratio %(1 μM)[c]
				A549	MDA-MB-231	MDA-MB-468		
1c	Br	H		10.54 ± 1.11	9.24 ± 2.07	8.32 ± 1.84	1.29	19.78 ± 0.48
2c	F	CH_3	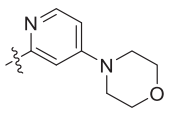	13.87 ± 1.45	13.19 ± 0.89	12.09 ± 0.52	3.83	19.22 ± 1.20
6c	F	H	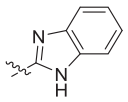	7.81 ± 1.62	5.03 ± 2.77	6.06 ± 2.25	0.83	22.34 ± 1.35
7c	Br	H	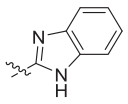	6.48 ± 1.72	3.38 ± 1.01	4.30 ± 1.82	0.304	25.67 ± 0.82
8c	Br	H	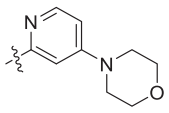	13.73 ± 1.97	9.21 ± 1.83	10.17 ± 1.79	2.45	20.99 ± 1.93
10c	Br	H		11.21 ± 2.58	8.11 ± 1.48	8.17 ± 2.01	4.84	17.20 ± 0.86
Rapamycin				30.72 ± 1.91	35.79 ± 1.38	37.20 ± 0.77	0.0008	31.03 ± 1.54
Temsirolimus				11.81 ± 2.46	17.57 ± 1.35	10.89 ± 1.73	2.29	15.33 ± 2.80

[a] Each compound was tested in triplicate; the data are presented as the mean ± SEM (n = 3).
[b] IC_{50} values obtained with cell viability assay for 24 h.
[c] Determined by flow cytometry analysis using MDC staining; the data are presented as the mean ± SEM (n = 3).

4.2. Cell viability determination

The cells were distributed into 96-well plates at a density of $5*10^3$ cells/well. After 24 h of incubation, the cells were treated with different concentrations of synthetic compounds within the specified time. Cell viability was measured by MTT assay.

4.3. Colony formation test

The proliferation potential of the cells was evaluated by plating 1000 cells in a 6-well plate. The plates were cultured at 37 °C for 14 days in a 5% CO_2 incubator. MDA-MB-231 and MDA-MB-468 cells fixed with 4% paraformaldehyde were stained with crystal violet. Data represents the mean ± SD of 3 independent experiments performed in three replicate wells.

4.4. GFP/mRFP-LC3 transfection

Incubate the MDA-MB-231 and MDA-MB-468 cells sequentially, starting with GFP/mRFP-LC3 transfection for 6 h. The transfected cells were then used for subsequent experiments after 24 h and analyzed under a fluorescence microscope.

4.5. Flow cytometry analysis

For Annexin V-FITC/PI staining, the treated cells were collected, washed twice with PBS, and then stained with Annexin V-FITC (1:1000) in binding buffer at room temperature in the dark. After 15 min, the cells were incubated with PI staining solution for 5 min. The cells were then measured by a flow cytometer (Becton Dickinson).

4.6. Western blot analysis

MDA-MB-231 and MDA-MB-468 cells were treated with **7c** for 24 h. The cells were then collected and lysed by lysis buffer at 4 °C for 30 min. After centrifugation at 12,000 rpm for 10 min, the protein level of the supernatant was quantified by the Bio-Rad DC protein assay (Bio-Rad Laboratories, Hercules, CA, USA). The same amount of total protein was separated by 12% SDS-PAGE, and then electrophoresed and transferred to PVDF membrane. Subsequently, the membrane was immersed in the blocking buffer. The primary antibody is used to detect the protein, then the HRP-conjugated secondary antibody is used to detect the protein, and ECL is used as the HRP substrate for visualization. Quantification of

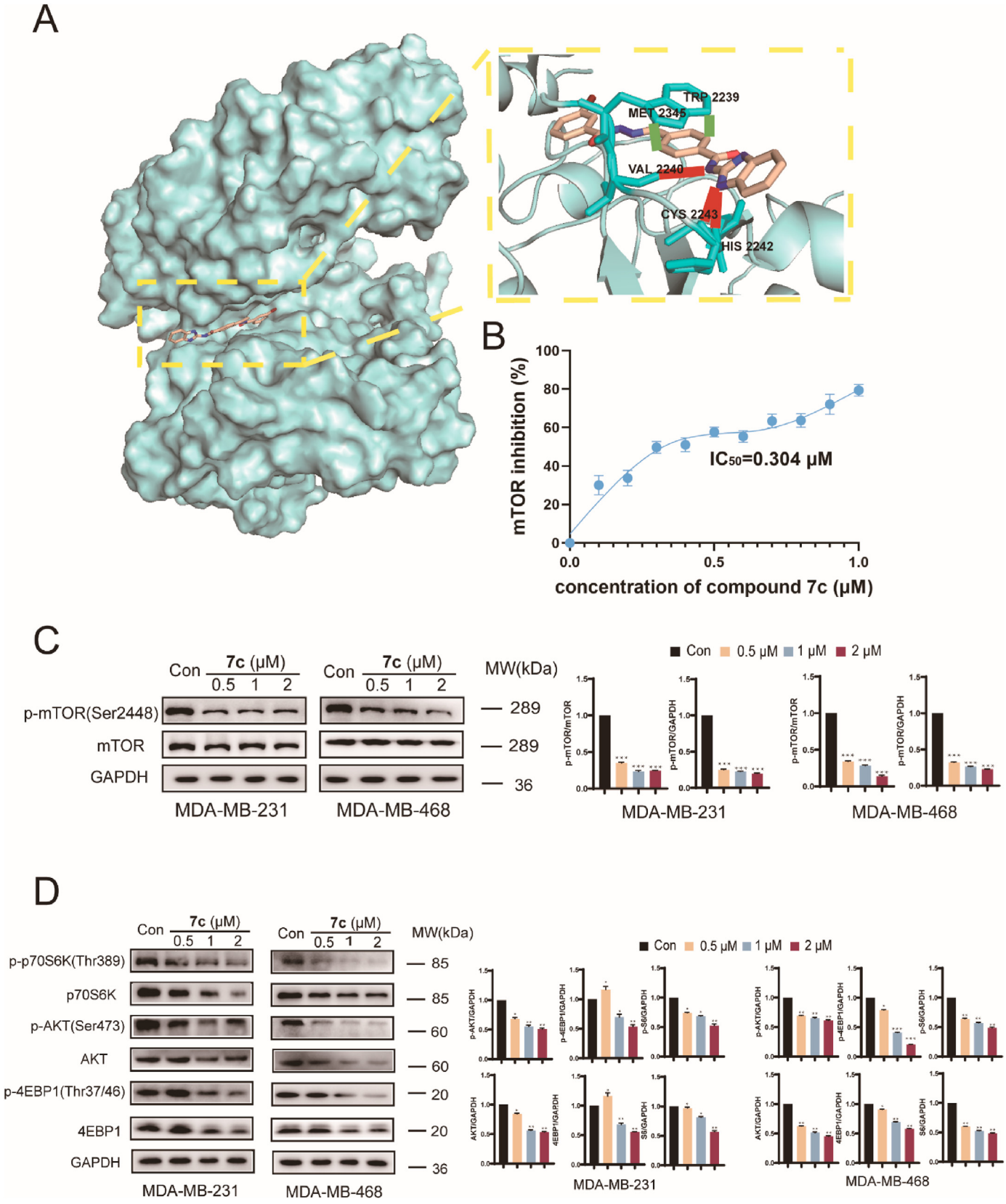

Fig. 2. Identification of **7c** as a new mTOR inhibitor. **A.** Predicted binding mode of compound **7c** in the active of mTOR (PDB ID: 4JT5). **B.** mTOR kinase inhibition rate curve of compound **7c**. **C.** Immunoblotting analysis of p-mTOR (Ser2448) and mTOR expression in MDA-MB-231 and MDA-MB-468 cells treated with the indicated concentrations of **7c** for 24 h. GAPDH was used as a loading control. Quantification of mTOR immunoblotting analysis were shown. Data are expressed as mean ± SEM. All data were representative of at least three independent experiments. *, $P < 0.05$, **, $P < 0.01$, ***, $P < 0.001$. Statistical significance compared with respective control groups. **D.** Immunoblotting analysis of p-p70S6K(Thr389), p70S6K, p-AKT(Ser473), AKT, p-4EBP1(Thr37/46), 4EBP1 expression in MDA-MB-231 and MDA-MB-468 cells treated with the indicated concentrations of **7c** for

immunoblotting was performed by Image Lab.

4.7. Molecular docking and pharmacophore model

All calculations are run using discovery Studio software (version 3.1). CHARMM force field is used to minimize the energy of ligand in docking procedure. The crystal structure of mTOR kinase (PDB Code: 4jt5) was obtained from PDB database. Choose the gold medal score as the score function. Identification of key pharmacodynamic characteristics is important for effective mTOR inhibitors. All the training set molecules were studied to find the common chemical characteristics of the reported mTOR inhibitors. The chemical characteristics of hydrogen bond acceptors, hydrogen bond donors, negative electricity centers and hydrophobic aromatic compounds were selected, and quantitative pharmacophore models were generated using corresponding statistical parameters (such as cost value, root mean square and fitting value). The best quality hypothesis is selected. The image was created using PyMOL.

4.8. Hoechst 33258 stain

The cells (5×10^4 per well) were treated with compound **7c** for 24 h. After washing twice with cold PBS, the cells were stained with Hoechst 33258 for 30 min in the dark at 37 °C. Then observe the morphological changes of the cells under a fluorescence microscope.

4.9. MDC staining

The MDA-MB-231 cells were treated with 1 μM compounds for 6 h, then coincubated with MDC (0.05 mM) at 37 °C for 30 min. Then, the MDC positive ratio was analyzed by flow cytometry (Becton Dickinson).

4.10. Statistical analysis

All the data and results presented have been confirmed in at least 3 independent experiments. The data are expressed as mean ± standard deviation and analyzed using GraphPad Prism 6.0. Statistical comparisons were made by one-way analysis of variance and SPSS 17.0 Student's *t*-test (Chicago, Illinois, USA). $P < 0.05$ was considered statistically significant.

4.11. Synthesis of compound A1, 1a-2a, 4a-8a, 11a, 13a-16a, 19a-25a, 1–14b, 1-10c

4.11.1. 3-bromo-N'-(4-hydroxybenzylidene)-4-methylbenzohydrazide (**A1**)

White powder; yield 82%; m.p. 182–183 °C; ^{1}H NMR (400 MHz, DMSO-d_6) δ 11.66 (s, 1H), 9.92 (s, 1H), 8.34 (s, 1H), 7.83 (d, J = 7.85 Hz, 1H), 7.56 (d, J = 8.44 Hz, 2H), 7.51 (d, J = 7.92 Hz, 1H), 6.84 (d, J = 8.44 Hz, 2H), 4.33 (t, J = 5.08 Hz, 1H), 2.42 (s, 3H); ^{13}C NMR (100 MHz, DMSO-d_6) δ 161.6, 160.0, 148.9, 141.6, 133.5, 131.6, 131.4, 129.4 (2C), 127.4, 125.7, 124.6, 116.2 (2C), 22.9; HRMS (ESI)$^+$: calcd for $C_{15}H_{13}BrN_2NaO_2$ [M + Na]$^+$: 355.0052, found: 355.0047.

4.11.2. 3-bromo-N'-(1-(4-hydroxyphenyl)ethylidene)-4-methylbenzohydrazide (**1a**)

White powder; yield 92%; m.p. 160–163 °C; ^{1}H NMR (400 MHz, DMSO-d_6) δ 10.70 (s, 1H), 9.78 (s, 1H), 8.07 (s, 1H), 7.80 (d, J = 7.41 Hz, 1H), 7.70 (d, J = 6.81 Hz, 2H), 7.49 (d, J = 7.91 Hz, 1H), 6.79 (d, J = 7.62 Hz, 2H), 2.42 (s, 3H), 2.29 (s, 2H); ^{13}C NMR (100 MHz, DMSO-d_6) δ 162.4, 159.5, 157.4, 141.3, 134.1, 131.6, 131.4, 129.3 (2C), 128.6, 127.6, 124.4, 115.6 (2C), 22.9, 15.0; HRMS (ESI)$^+$: calcd for $C_{16}H_{15}BrN_2NaO_2$ [M + Na]$^+$: 369.0209, found: 369.0214.

4.11.3. N'-(1-(4-aminophenyl) ethylidene)-3-bromo-4-methylbenzohydrazide (**2a**)

White powder; yield 79%; m.p. 154–155 °C; ^{1}H NMR (400 MHz, DMSO-d_6) δ 10.61 (s, 1H), 8.07 (s, 1H), 7.80 (d, J = 7.69 Hz, 1H), 7.57 (d, J = 7.71 Hz, 2H), 7.48 (d, J = 7.92 Hz, 1H), 6.56 (d, J = 7.92 Hz, 2H), 5.49 (s, 2H), 2.41 (s, 3H), 2.24 (s, 2H); ^{13}C NMR (100 MHz, DMSO-d_6) δ 162.1, 158.4, 151.0, 141.2, 134.3, 131.5 (2C), 131.4, 128.3, 127.5, 125.4, 124.4, 113.6 (2C), 22.9, 14.8; HRMS (ESI)$^+$: calcd for $C_{16}H_{16}BrN_3NaO$ [M + Na]$^+$: 368.0369, found: 368.0367.

4.11.4. 3-bromo-N'-(1-(3,5-dihydroxyphenyl)ethylidene) benzohydrazide (**4a**)

White powder; yield 87%; m.p. 156–158 °C; ^{1}H NMR (400 MHz, DMSO-d_6) δ 10.78 (s,1H), 9.34 (s,2H), 8.04 (s,1H), 7.87 (d, J = 5.94 Hz, 1H), 7.78 (d, J = 7.57 Hz, 1H), 7.48 (t, J = 7.72 Hz, 1H), 6.72 (s, 2H), 6.26 (s, 1H), 2.26 (s, 3H); ^{13}C NMR (100 MHz, DMSO-d_6) δ 162.3, 158.5 (2C), 151.0, 140.2, 136.9, 136.5, 130.9, 128.3, 127.6, 125.3, 111.7 (2C),95.1, 14.8; HRMS (ESI)$^+$: calcd for $C_{15}H_{13}BrN_2NaO_3$ [M + Na]$^+$: 371.0002, found: 371.0001.

4.11.5. N'-(1-(4-aminophenyl)ethylidene)-3-bromobenzohydrazide (**5a**)

White powder; yield 90%; m.p. 176–178 °C; ^{1}H NMR (400 MHz, DMSO-d_6) δ 10.67 (s, 1H), 8.03 (s, 1H), 7.87 (d, J = 7.31 Hz, 1H), 7.76 (d, J = 7.31 Hz, 1H), 7.58 (d, J = 7.82 Hz, 2H), 7.46 (t, J = 7.76 Hz, 1H), 6.56 (d, J = 8.33 Hz, 1H), 5.51 (s, 2H), 2.24 (s, 3H); ^{13}C NMR (100 MHz, DMSO-d_6) δ 162.3, 158.6, 151.1, 137.0, 134.4, 131.0, 130.7, 128.3 (2C), 127.3, 125.3, 122.1, 113.6 (2C), 14.8; HRMS (ESI)$^+$: calcd for $C_{15}H_{14}BrN_3NaO$ [M + Na]$^+$: 354.0212, found: 354.0212.

4.11.6. 3-Bromo-N-(4-hydroxyphenethyl)-4-methylbenzamide (**6a**)

White powder; yield 77%; m.p. 159–162 °C; ^{1}H NMR (400 MHz, DMSO-d_6) δ 9.15 (s, 1H), 8.56 (t, J = 5.51 Hz, 1H), 8.02 (d, J = 1.54 Hz, 1H), 7.74 (dd, J = 7.87 Hz, 1.64 Hz, 1H), 7.44 (d, J = 8.00 Hz, 1H), 7.01 (d, J = 8.33 Hz, 2H), 6.67 (d, J = 8.40 Hz, 2H), 3.40 (m, 2H), 2.71 (t, J = 7.53 Hz, 2H), 2.38 (s, 3H); ^{13}C NMR (100 MHz, DMSO-d_6) δ 164.11, 156.1, 140.9, 134.6, 133.2, 132.9, 131.1, 130.0 (2C), 126.9, 124.5, 115.6 (2C), 41.8, 34.7, 22.8; HRMS (ESI)$^+$: calcd for $C_{16}H_{16}BrNNaO_2$ [M + Na]$^+$: 356.0256, found: 356.0259.

4.11.7. 3-Bromo-N-(4-hydroxybenzyl)-4-methylbenzamide (**7a**)

White powder; yield 84%; m.p. 166–167 °C; ^{1}H NMR (400 MHz, DMSO-d_6) δ 9.25 (s, 1H), 8.96 (t, J = 5.83 Hz, 1H), 8.09 (d, J = 1.62 Hz, 1H), 7.80 (dd, J = 7.89 Hz, 1.66 Hz, 1H), 7.45 (d, J = 7.96 Hz, 1H), 7.12 (d, J = 8.50 Hz, 2H), 6.71 (d, J = 8.47 Hz, 2H), 4.34 (d, J = 5.90 Hz, 2H), 2.39 (s, 3H); ^{13}C NMR (100 MHz, DMSO-d_6) δ 164.8, 156.7, 141.0, 134.4, 131.4, 131.2, 130.1 (2C), 129.2, 127.1, 124.5, 115.5 (2C), 42.7, 22.8; HRMS (ESI)$^+$: calcd for $C_{15}H_{14}BrNNaO_2$ [M + Na]$^+$: 342.0100, found: 342.0101.

4.11.8. 3-bromo-4-methyl-N'-(1-(4-(trifluoromethyl)phenyl) ethylidene)benzohydrazide (**8a**)

White powder; yield 81%; m.p. 170–172 °C; ^{1}H NMR (400 MHz, DMSO-d_6) δ 10.94 (s, 1H), 8.10 (s, 1H), 8.02 (s, 2H), 7.82 (s, 2H), 7.77 (s, 1H), 7.50 (d, J = 7.80 Hz, 1H), 2.44 (s, 3H), 2.40 (s, 3H); ^{13}C NMR (100 MHz, DMSO-d_6) δ 142.4, 133.8, 131.9, 131.4, 127.6, 126.0, 125.8

24 h. GAPDH was used as a loading control. Quantification of mTOR pathway immunoblotting analysis were shown. Data are expressed as mean ± SEM. All data were representative of at least three independent experiments. *, $P < 0.05$, **, $P < 0.01$, ***, $P < 0.001$. Statistical significance compared with respective control groups.

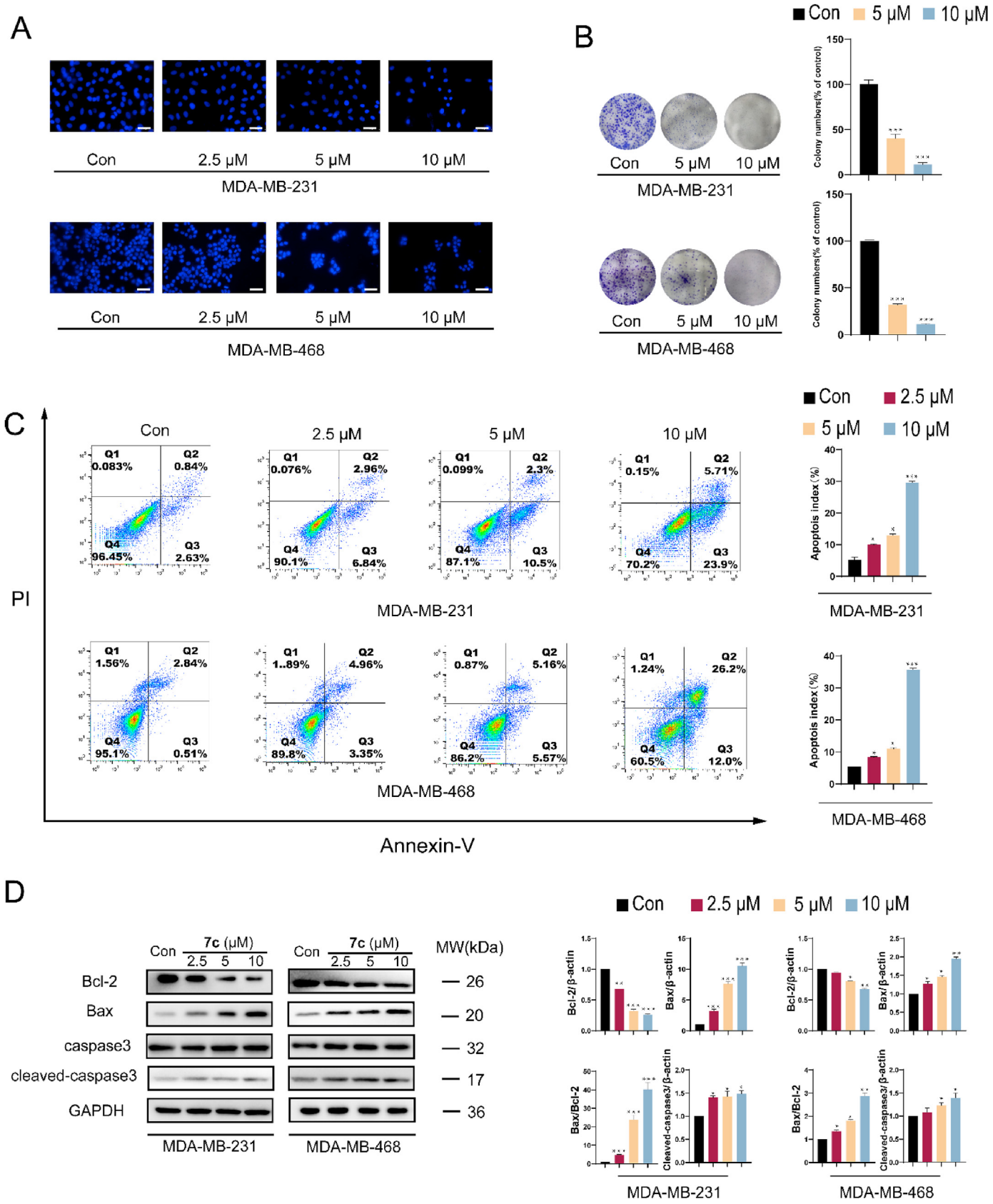

Fig. 3. **7c** inhibits colony formation and promotes cell apoptosis in MDA-MB-231 and MDA-MB-468 cells. **A.** Hoechst 33258 staining assay of MDA-MB-231 and MDA-MB-468 cells treated with or without **7c** (2.5 μM, 5 μM or 10 μM) with Scale bar: 50 μm. **B.** Colony formation assay of MDA-MB-231 and MDA-MB-468 cells treated with or without **7c** (5 μM or 10 μM). Representative images and quantification of colonies were shown. Data are expressed as mean ± SEM. All data were representative of at least three independent experiments. *, $P < 0.05$, **, $P < 0.01$, ***, $P < 0.001$. Statistical significance compared with respective control groups.**C.** MDA-MB-231 and MDA-MB-468 cells were treated with or

(2C), 125.7, 124.4 (2C), 123.3 (2C), 22.9, 15.1; HRMS (ESI)$^+$: calcd for $C_{17}H_{14}BrF_3N_2NaO$ [M + Na]$^+$: 421.0134, found: 421.0131.

*4.11.9. 3-bromo-4-methyl-N'-(1-(pyridin-4-yl)ethylidene) benzohydrazide (**9a**)*

White powder; yield 76%; m.p. 162–163 °C; ^{1}H NMR (400 MHz, DMSO-d_6) δ 10.98 (s, 1H), 8.63 (s, 2H), 8.08 (s, 1H), 7.77 (m, 3H), 7.51 (d, J = 7.93 Hz, 1H), 2.43 (s, 3H), 2.38 (s, 3H); ^{13}C NMR (100 MHz, DMSO-d_6) δ 162.0, 158.4, 151.0, 144.7, 138.0, 134.0, 130.1, 128.3 (2C), 125.4, 113.6 (2C), 101.5, 28.0, 14.8; HRMS (ESI)$^+$: calcd for $C_{15}H_{14}BrN_3NaO$ [M + Na]$^+$: 354.0212, found: 354.0214.

*4.11.10. 3-iodo-4-methyl-N'-(1-(4-(trifluoromethyl)phenyl) ethylidene)benzohydrazide (**11a**)*

White powder; yield 84%; m.p. 174–175 °C; ^{1}H NMR (400 MHz, DMSO-d_6) δ 10.93 (s, 1H), 8.31 (s, 1H), 8.03 (s, 2H), 7.81 (m, 3H), 7.48 (d, J = 7.89 Hz, 1H), 2.45 (s, 3H), 2.40 (s, 3H); ^{13}C NMR (100 MHz, DMSO-d_6) δ 162.9, 154.1, 145.2, 142.4, 138.2, 133.6, 130.1, 128.7, 128.5, 127.6, 125.7(J = 3.71 Hz), 125.7(J = 3.62 Hz), 123.3(J = 272.15 Hz), 120.6, 101.4, 28.0, 15.1; HRMS (ESI)$^+$: calcd for $C_{17}H_{14}F_3IN_2NaO$ [M + Na]$^+$: 468.9995, found: 468.9994.

*4.11.11. N'-(1-(2,4-dihydroxyphenyl)ethylidene)-3-fluorobenzohydrazide (**13a**)*

White powder; yield 87%; m.p. 190–191 °C; ^{1}H NMR (400 MHz, DMSO-d_6) δ 14.80 (s, 1H), 7.81 (d, J = 7.94 Hz, 1H), 7.74 (d, J = 10.01 Hz, 1H), 7.50 (m, 1H), 7.35 (m, 2H), 6.20 (d, J = 9.10 Hz, 1H), 6.17 (s, 1H), 2.44 (s, 3H); ^{13}C NMR (100 MHz, DMSO-d_6) δ 162.3, 158.6, 151.1, 137.0, 134.4, 131.0, 130.7, 128.3 (2C), 127.3, 125.3, 122.1, 113.6 (2C), 14.8; HRMS (ESI)$^+$: calcd for $C_{15}H_{13}FN_2NaO_3$ [M + Na]$^+$: 311.0802, found: 311.0802.

*4.11.12. N'-(1-(4-aminophenyl)ethylidene)-3-iodo-4-methylbenzohydrazide (**14a**)*

White powder; yield 79%; m.p. 167–169 °C; ^{1}H NMR (400 MHz, DMSO-d_6) δ 10.58 (s, 1H), 8.30 (s, 1H), 7.81 (d, J = 7.04 Hz, 1H), 7.57 (d, J = 7.70 Hz, 2H), 7.44 (d, J = 8.02 Hz, 1H), 6.56 (d, J = 8.02 Hz, 2H), 5.48 (s, 2H), 2.43 (s, 3H), 2.23 (s, 3H); ^{13}C NMR (100 MHz, DMSO-d_6) δ 162.0, 158.4, 151.0, 144.7, 138.0, 134.0, 130.1 (2C), 128.3, 128.0, 125.4, 113.6 (2C), 101.5, 28.0, 14.8; HRMS (ESI)$^+$: calcd for $C_{16}H_{16}IN_3NaO$ [M + Na]$^+$: 416.0230, found: 416.0238.

*4.11.13. N'-(1-(4-aminophenyl)ethylidene)-3-iodobenzohydrazide (**15a**)*

White powder; yield 86%; m.p. 184–185 °C; ^{1}H NMR (400 MHz, DMSO-d_6) δ 10.65 (s, 1H), 8.19 (s, 1H), 7.92 (d, J = 7.51 Hz, 1H), 7.87 (d, J = 7.51 Hz, 1H), 7.58 (d, J = 7.85 Hz, 2H), 7.30 (t, J = 7.78 Hz, 1H), 6.56 (d, J = 8.03 Hz, 2H), 5.49 (s, 2H), 2.24 (s, 3H); ^{13}C NMR (100 MHz, DMSO-d_6) δ 162.3, 158.5, 151.0, 140.2, 136.9, 136.5, 130.9, 128.3 (2C), 127.6, 125.3, 114.8 (2C), 95.1, 14.8; HRMS (ESI)$^+$: calcd for $C_{15}H_{14}IN_3NaO$ [M + Na]$^+$: 402.0074, found: 402.0079.

*4.11.14. N'-(1-(4-aminophenyl)ethylidene)-3-fluoro-4-methylbenzohydrazide (**16a**)*

White powder; yield 80%; m.p. 173–175 °C; ^{1}H NMR (400 MHz, DMSO-d_6) δ 10.54 (s, 1H), 7.64 (d, J = 8.74 Hz, 2H), 7.57 (d, J = 7.63 Hz, 2H), 7.41 (t, J = 7.84 Hz, 1H), 6.57 (d, J = 8.08 Hz, 2H), 5.49 (s, 2H), 2.30 (s, 3H), 2.24 (s, 3H); ^{13}C NMR (100 MHz, DMSO-d_6) δ 162.1, 158.4, 151.0, 141.2, 134.3, 131.5, 131.4, 128.3 (2C), 127.5, 125.4, 124.4, 113.6 (2C), 22.9, 14.8; HRMS (ESI)$^+$: calcd for $C_{16}H_{16}FN_3NaO$ [M + Na]$^+$: 308.1169, found: 308.1170.

*4.11.15. 4-(1-(2-(3-bromobenzoyl)hydrazono)ethyl)benzoic acid (**19a**)*

White powder; yield 91%; m.p. 146–147 °C; ^{1}H NMR (400 MHz, DMSO-d_6) δ 13.01 (s, 1H), 10.96 (s, 1H), 8.07 (s, 1H), 7.98 (s, 3H), 7.88 (s, 1H), 7.79 (d, J = 7.73 Hz, 1H), 7.49 (t, J = 7.88 Hz, 1H), 2.41 (s, 3H); ^{13}C NMR (100 MHz, DMSO-d_6) δ 167.5, 163.2, 154.11, 142.4 (2C), 136.6, 134.8, 131.8, 131.0, 129.8 (2C), 127.6, 127.3, 127.0, 122.0, 15.2; HRMS (ESI)$^+$: calcd for $C_{16}H_{13}BrN_2NaO_3$ [M + Na]$^+$: 383.0002, found: 383.0006.

*4.11.16. 4-(1-(2-(3-iodobenzoyl)hydrazono)ethyl)benzoic acid (**20a**)*

White powder; yield 77%; m.p. 165–168 °C; ^{1}H NMR (400 MHz, DMSO-d_6) δ 13.03 (s, 1H), 10.94 (s, 1H), 8.21 (s, 1H), 7.95 (m, 6H), 7.33 (t, J = 7.78 Hz, 1H), 2.40 (s, 3H); ^{13}C NMR (100 MHz, DMSO-d_6) δ 167.5, 163.2, 154.8, 142.5 (2C), 140.6, 136.7, 136.5, 131.8, 130.9, 129.8 (2C), 127.9, 127.0, 95.1, 15.1; HRMS (ESI)$^+$: calcd for $C_{16}H_{13}IN_2NaO_3$ [M + Na]$^+$: 430.9863, found: 430.9861.

*4.11.17. 3-iodo-4-methyl-N'-(1-(pyridin-4-yl)ethylidene) benzohydrazide (**21a**)*

White powder; yield 74%; m.p. 157–158 °C; ^{1}H NMR (400 MHz, DMSO-d_6) δ 10.97 (s, 1H), 8.64 (d, J = 4.05 Hz, 2H), 8.31 (s, 1H), 7.77 (m, 3H), 7.48 (d, J = 7.94 Hz, 1H), 2.45 (s, 3H), 2.37 (s, 3H); ^{13}C NMR (100 MHz, DMSO-d_6) δ 163.3, 153.1, 150.5, 145.5 (2C), 140.7, 136.8, 136.3, 130.9, 128.0, 121.1, 121.0 (2C), 95.1, 14.6; HRMS (ESI)$^+$: calcd for $C_{15}H_{14}IN_3NaO$ [M + Na]$^+$: 402.0074, found: 402.0078.

*4.11.18. 3-iodo-N'-(1-(pyridin-4-yl)ethylidene)benzohydrazide (**22a**)*

White powder; yield 88%; m.p. 159–160 °C; ^{1}H NMR (400 MHz, DMSO-d_6) δ 11.02 (s, 1H), 8.64 (s, 2H), 8.20 (s, 1H), 7.96 (d, J = 7.64 Hz, 1H), 7.88 (s, 1H), 7.75 (s, 2H), 7.33 (t, J = 7.79 Hz, 1H), 2.37 (s, 3H); ^{13}C NMR (100 MHz, DMSO-d_6) δ 163.3, 153.1, 150.5 (2C), 145.5, 140.7, 136.8, 136.3, 130.9, 128.0, 121.0 (2C), 95.1, 14.6; HRMS (ESI)$^+$: calcd for $C_{14}H_{12}IN_3NaO$ [M + Na]$^+$: 387.9917, found: 387.9926.

*4.11.19. 3-Bromo-4-methyl-N-(quinolin-2-yl)benzamide (**23a**)*

White powder; yield 83%; m.p. 150–152 °C; ^{1}H NMR (400 MHz, DMSO-d_6) δ 11.23 (s, 1H), 8.42 (d, J = 9.02 Hz, 1H), 8.32 (d, J = 9.10 Hz, 2H), 8.01 (m, 1H), 7.96 (d, J = 8.02 Hz, 1H), 7.89 (d, J = 8.34 Hz, 1H), 7.75 (d, J = 7.70 Hz, 1H), 7.53 (m, 2H), 2.43 (s, 3H); ^{13}C NMR (100 MHz, DMSO-d_6) δ 165.4, 152.1, 146.6, 142.2, 138.8, 133.8, 132.2, 131.5, 130.6, 128.3, 127.9, 127.4, 126.3, 125.8, 124.5, 115.9, 23.0; HRMS (ESI)$^+$: calcd for $C_{17}H_{13}BrN_2NaO$ [M + Na]$^+$: 363.0103, found: 363.0103.

*4.11.20. 3-Bromo-N-(isoquinolin-3-yl)-4-methylbenzamide (**24a**)*

White powder; yield 78%; m.p. 168–169 °C; ^{1}H NMR (400 MHz, DMSO-d_6) δ 10.99 (s, 1H), 9.22 (s, 1H), 8.62 (s, 1H), 8.31 (d, J = 1.66 Hz, 1H), 8.10 (d, J = 8.14 Hz, 1H), 8.01 (dd, J = 7.90 Hz, 1.66 Hz, 1H), 7.96 (d, J = 8.32 Hz, 1H), 7.75 (m, 1H), 7.58 (m, 1H), 7.52 (d, J = 7.94 Hz, 1H), 2.43 (s, 3H); ^{13}C NMR (100 MHz, DMSO-d_6)

without **7c** (2.5 μM, 5 μM, 10 μM) for 24 h, and apoptosis ratios were determined by flow cytometry analysis of Annexin-V/PI double staining. Representative images and quantification of apoptosis were shown. Data are expressed as mean ± SEM. All data were representative of at least three independent experiments. *, $P < 0.05$, **, $P < 0.01$, ***, $P < 0.001$. Statistical significance compared with respective control groups. **D.** Immunoblotting analysis of Bcl-2, Bax, caspase3 and cleaved-caspase3 expression in MDA-MB-231 and MDA-MB-468 cells treated with the indicated concentrations of **7c** for 24 h. GAPDH was used as a loading control. Quantification of immunoblotting analysis were shown. Quantification of mTOR immunoblotting analysis were shown. Data are expressed as mean ± SEM. All data were representative of at least three independent experiments. *, $P < 0.05$, **, $P < 0.01$, ***, $P < 0.001$. Statistical significance compared with respective control groups.

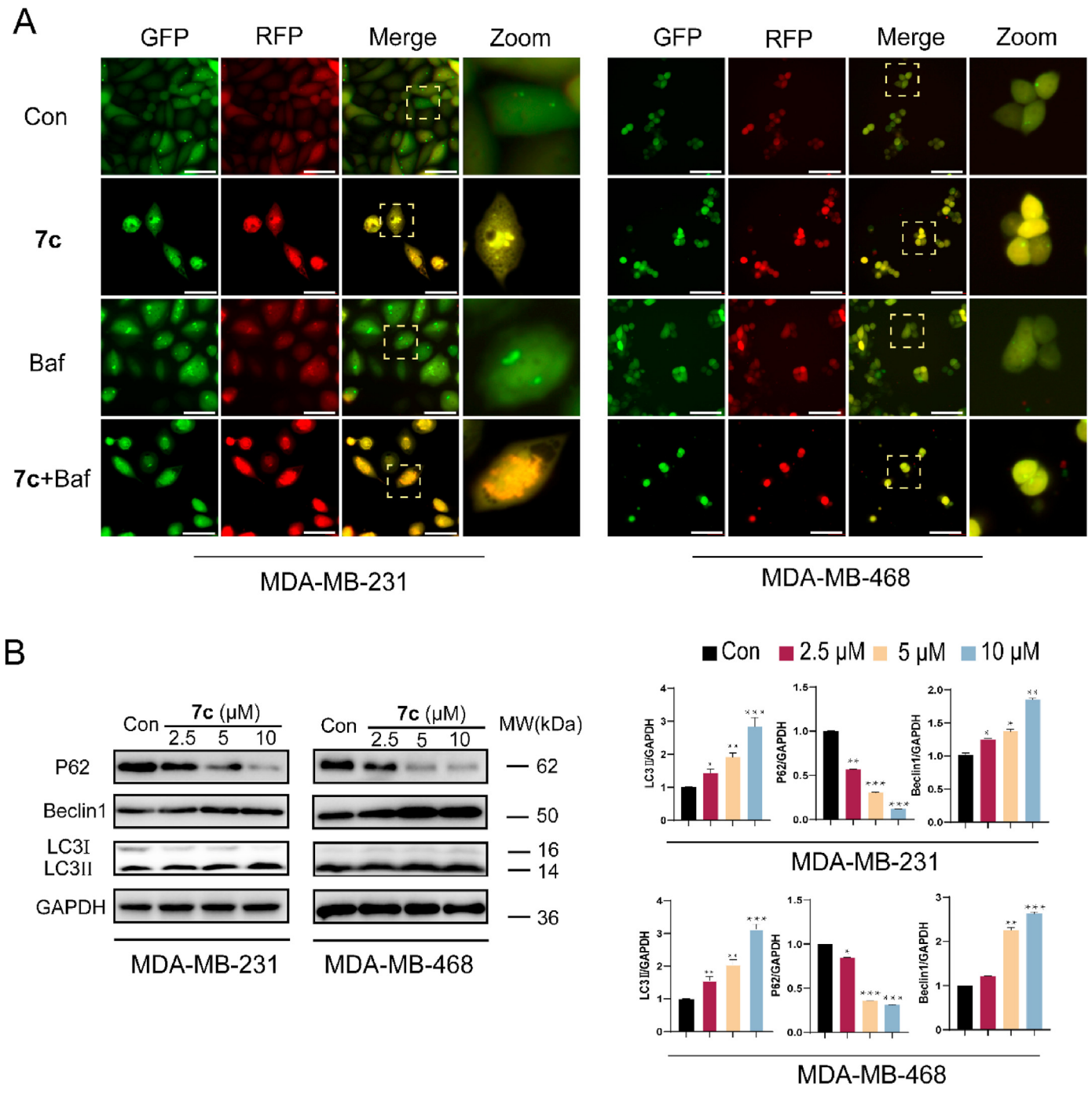

Fig. 4. 7c can induce autophagy in MDA-MB-231 and MDA-MB-468 cells. **A.** MDA-MB-231 and MDA-MB-468 cells were transfected with GFP/mRFP-LC3 plasmid, after co-incubation with **7c** (5 μM) in the presence or absence of BafA1 (10 nM). Representative images and quantitative analysis of LC3 puncta were shown. Scale bar, 20 μm. **B.** Immunoblotting analysis of p62, Beclin-1, LC3 expression in MDA-MB-231 and MDA-MB-468 cells treated with the indicated concentrations of **7c** for 24 h. GAPDH was used as a loading control. Quantification of immunoblotting analysis were shown. Quantification of mTOR immunoblotting analysis were shown. Data are expressed as mean ± SEM. All data were representative of at least three independent experiments. *, $P < 0.05$, **, $P < 0.01$, ***, $P < 0.001$. Statistical significance compared with respective control groups.

δ 164.6, 151.7, 147.6, 141.9, 137.6, 134.2, 132.0, 131.4, 131.4, 128.0, 127.7, 127.0, 126.5, 126.5, 124.5, 108.8, 22.9; HRMS (ESI)$^+$: calcd for $C_{17}H_{13}BrN_2NaO$ [M + Na]$^+$: 363.0103, found: 363.0091.

*4.11.21. N-(1H-benzo[d]imidazole-2-yl)-4-(trifluoromethoxy) benzamide (**25a**)*

White powder; yield 76%; m.p. 157–160 °C; ^{1}H NMR (400 MHz, DMSO-d_6) δ 12.57 (s, 1H), 8.51 (s, 1H), 8.31 (d, J = 8.72 Hz, 1H), 8.07 (d, J = 8.72 Hz, 1H), 7.58 (m, 2H), 7.49 (d, J = 8.28 Hz, 1H), 7.37 (m, 1H), 7.28 (m, 1H), 7.21 (m, 1H); ^{13}C NMR (100 MHz, DMSO-d_6) δ 166.6, 151.6 (J = 32.17 Hz), 151.0, 133.5, 132.2 (2C), 131.4 (2C), 130.3, 130.0, 123.6, 123.4, 121.2, 121.1, 113.5, 111.8; HRMS (ESI)$^+$: calcd for $C_{15}H_{10}F_3N_3NaO_2$ [M + Na]$^+$: 344.0617, found: 344.0625.

*4.11.22. 1-(3-bromobenzyl)-3-(4-(trifluoromethyl)phenyl)urea (**1b**)*

White powder; yield 94%; m.p. 164–165 °C; ^{1}H NMR (400 MHz,

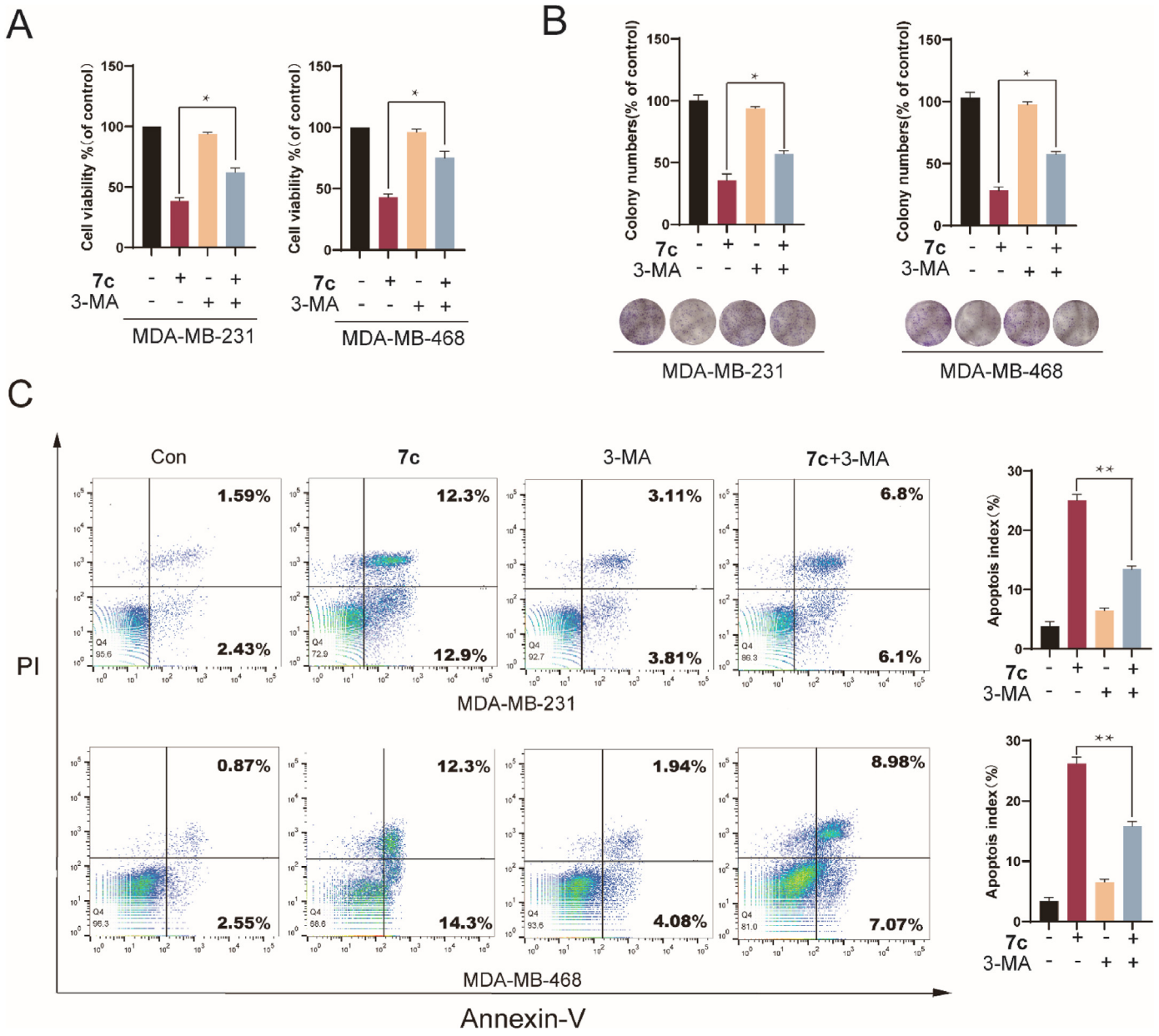

Fig. 5. **7c** can induce autophagic cell death in TNBC cells. **A.** MDA-MB-231 and MDA-MB-468 cells were treated with **7c** (5 μM) alone or in combination with 3-MA (1 mM) for 24 h, 3-MA was added 1 h before treatment of **7c**. After treatment, cell viability was measured by MTT assay. **B.** Colony formation assay of MDA-MB-231 and MDA-MB-468 cells treated with **7c** (10 μM) alone or in combination with 3-MA (1 mM). Representative images and quantification of colonies were shown. **C.** MDA-MB-231 and MDA-MB-468 cells were treated with **7c** (10 μM) alone or in combination with 3-MA (1 mM) for 24 h, and apoptosis ratios were determined by flow cytometry analysis of Annexin-V/PI double staining. 3-MA was added 1 h before treatment of **7c**. Representative images and quantification of apoptosis were shown. Data are expressed as mean ± SEM. All data were representative of at least three independent experiments. *, $P < 0.05$, **, $P < 0.01$, ***, $P < 0.001$. Statistical significance compared with respective control groups.

DMSO-d_6) δ 9.06 (s, 1H), 7.59 (m, 4H), 7.50 (s, 1H), 7.44 (m, 1H), 7.31 (m, 2H), 6.85 (t, J = 5.95 Hz, 1H), 4.31 (d, J = 5.98 Hz, 2H); ^{13}C NMR (100 MHz, DMSO-d_6) δ 155.4, 144.6, 143.6, 131.0, 130.3 (J = 22.17 Hz), 126.7 (J = 3.65 Hz), 126.4 (J = 3.65 Hz), 126.4, 122.1 (2C), 121.5 (J = 230.11 Hz, 2C), 117.8 (2C), 42.7; HRMS (ESI)$^+$: calcd for $C_{15}H_{12}BrF_3N_2NaO$ [M + Na]$^+$: 394.9977, found: 394.9983.

*4.11.23. 1-Benzyl-1-methyl-3-(4-(trifluoromethyl)phenyl)urea (**2b**)*

White powder; yield 92%; m.p. 161–164 °C; ^{1}H NMR (400 MHz, DMSO-d_6) δ 8.80 (s, 1H), 7.74 (d, J = 8.52 Hz, 2H), 7.59 (d, J = 8.52 Hz, 2H), 7.36 (m, 2H), 7.27 (m, 3H), 4.57 (s, 2H), 2.94 (s, 3H); ^{13}C NMR (100 MHz, DMSO-d_6) δ 155.7, 144.11, 138.6, 129.0, 127.8, 127.5 (2C), 126.0 (J = 3.77 Hz), 126.0 (J = 3.77 Hz), 123.8 (J = 271.13 Hz, 2C), 122.3 (J = 32.37 Hz), 119.6 (2C), 51.8, 34.1; HRMS (ESI)$^+$: calcd for $C_{16}H_{15}F_3N_2NaO$ [M + Na]$^+$: 331.1028, found: 331.1028.

*4.11.24. 1-(4-hydroxybenzyl)-3-(4-(trifluoromethyl)phenyl)urea (**3b**)*

White powder; yield 94%; m.p. 179–181 °C; ^{1}H NMR (400 MHz, DMSO-d_6) δ 9.26 (s, 1H), 8.90 (s, 1H), 7.58 (m, 4H), 7.12 (s, 1H), 7.09 (s, 1H), 6.73 (s, 1H), 6.70 (s, 1H), 6.61 (t, J = 5.64 Hz, 1H), 4.18 (d, J = 5.78 Hz, 2H); ^{13}C NMR (100 MHz, DMSO-d_6) δ 156.8, 155.2, 144.7, 130.5 (2C), 129.1 (2C), 126.4 (J = 3.60 Hz), 126.4 (J = 3.60 Hz), 121.3 (J = 31.85 Hz), 117.7 (2C), 115.5 (2C), 42.8; HRMS (ESI)$^+$: calcd for $C_{15}H_{13}F_3N_2NaO_2$ [M + Na]$^+$: 333.0821, found: 333.0817.

*4.11.25. 1-(3-chlorophenyl)-3-(4-hydroxybenzyl)urea (**4b**)*

White powder; yield 95%; m.p. 184–186 °C; ^{1}H NMR (400 MHz, DMSO-d_6) δ 9.26 (s, 1H),8.68 (s, 1H),7.68 (t, J = 1.89 Hz, 1H),7.21 (m, 2H), 7.10 (d, J = 8.26 Hz, 2H), 6.93 (m, 1H), 6.71 (d, J = 8.26 Hz, 2H), 6.54 (t, J = 5.73 Hz, 1H), 4.17 (d, J = 5.73 Hz, 2H); ^{13}C NMR (100 MHz, DMSO-d_6) δ 156.7, 155.4, 142.5, 133.6, 130.7, 130.6, 129.0 (2C), 121.1, 117.4, 116.5, 115.5 (2C), 42.8; HRMS (ESI)$^+$: calcd for $C_{14}H_{13}ClN_2NaO_2$ [M + Na]$^+$: 299.0558, found: 299.0561.

*4.11.26. 1-(3-fluorophenyl)-3-(4-hydroxybenzyl)urea (**5b**)*

White powder; yield 97%; m.p. 167–169 °C; ^{1}H NMR (400 MHz, DMSO-d_6) δ 9.26 (s, 1H), 8.70 (s, 1H), 7.46 (m, 1H), 7.23 (q, J = 7.78 Hz, 1H), 7.10 (d, J = 8.41 Hz, 2H), 7.02 (dd, J = 8.20 Hz, 1.30 Hz, 1H), 6.70 (m, 3H), 6.53 (t, J = 5.80 Hz, 1H), 4.17 (d, J = 5.73 Hz, 2H); ^{13}C NMR (100 MHz, DMSO-d_6) δ 164.1 (J = 240.96 Hz), 156.7, 155.4, 142.9, 142.8, 130.6, 130.5, 129.0, 115.5 (2C), 113.8 (J = 2.53 Hz), 107.6 (J = 21.42 Hz), 104.6 (J = 26.64 Hz), 42.8; HRMS (ESI)$^+$: calcd for $C_{14}H_{13}FN_2NaO_2$ [M + Na]$^+$: 283.0853, found: 283.0851.

*4.11.27. 1-(3-chlorophenyl)-3-(1-phenylethyl)urea (**6b**)*

White powder; yield 90%; m.p. 185–186 °C; ^{1}H NMR (400 MHz, DMSO-d_6) δ 8.61 (s, 1H), 7.64 (t, J = 1.97 Hz, 1H), 7.34 (s, 2H), 7.33 (s, 2H), 7.22 (m, 2H), 7.14 (m, 1H), 6.92 (m, 1H), 6.72 (q, J = 7.84 Hz, 1H), 4.81 (m, 1H), 1.39 (d, J = 6.97 Hz, 3H); ^{13}C NMR (100 MHz, DMSO-d_6) δ 154.6, 145.5, 133.6, 130.7, 128.8 (2C), 127.2, 126.3 (2C), 121.1, 117.4, 117.3, 116.4, 49.1, 23.4; HRMS (ESI)$^+$: calcd for $C_{15}H_{15}ClN_2NaO$ [M + Na]$^+$: 297.0765, found: 297.0767.

*4.11.28. 1-(3-fluorophenyl)-3-(1-phenylethyl)urea (**7b**)*

White powder; yield 95%; m.p. 179–181 °C; ^{1}H NMR (400 MHz, DMSO-d_6) δ 8.63 (s, 1H), 7.43 (m, 1H), 7.36 (s, 2H), 7.33 (s, 2H), 7.23 (m, 2H), 7.00 (m, 1H), 6.70 (m, 2H), 4.82 (m, 1H), 1.39 (d, J = 6.96 Hz, 3H); ^{13}C NMR (100 MHz, DMSO-d_6) δ 161.7 (J = 239.31 Hz), 154.6, 145.5, 142.7 (J = 11.72 Hz), 130.6, 130.5 (J = 10.28 Hz, 2C), 128.8, 127.2, 126.3 (2C), 113.7 (J = 2.86 Hz), 107.7 (J = 21.31 Hz), 104.8 (J = 27.21 Hz), 49.1, 23.4; HRMS (ESI)$^+$: calcd for $C_{15}H_{15}FN_2NaO$ [M + Na]$^+$: 281.1060, found: 281.1066.

*4.11.29. 1-(1-phenylethyl)-3-(p-tolyl)urea (**8b**)*

White powder; yield 93%; m.p. 176–178 °C; ^{1}H NMR (400 MHz, DMSO-d_6) δ 8.24 (s, 1H), 7.34 (s, 2H), 7.32 (s, 2H), 7.23 (m, 3H), 7.00 (d, J = 8.34 Hz, 2H), 6.53 (d, J = 7.87 Hz, 1H), 4.81 (m, 1H), 2.19 (s, 3H), 1.38 (d, J = 7.01 Hz, 3H); ^{13}C NMR (100 MHz, DMSO-d_6) δ 154.11, 145.7, 138.3, 130.2, 129.5, 128.8, 127.1, 126.3, 118.1, 49.0, 23.6, 20.7; HRMS (ESI)$^+$: calcd for $C_{16}H_{18}N_2NaO$ [M + Na]$^+$: 277.1311, found: 277.1315.

*4.11.30. 1-(4-hydroxybenzyl)-3-(p-tolyl)urea (**9b**)*

White powder; yield 96%; m.p. 192–194 °C; ^{1}H NMR (400 MHz, DMSO-d_6) δ 9.25 (s, 1H), 8.31 (s, 1H), 7.26 (d, J = 8.33 Hz, 2H), 7.10 (d, J = 8.33 Hz, 2H), 7.02 (d, J = 8.24 Hz, 2H), 6.71 (d, J = 8.49 Hz, 2H), 6.37 (t, J = 5.74 Hz, 1H), 4.15 (d, J = 5.72 Hz, 2H), 2.21 (s, 3H); ^{13}C NMR (100 MHz, DMSO-d_6) δ 156.7, 155.7, 138.4, 130.9, 130.2, 129.5 (2C), 129.0 (2C), 118.2 (2C), 115.5 (2C), 42.8, 20.8; HRMS (ESI)$^+$: calcd for $C_{15}H_{16}N_2NaO_2$ [M + Na]$^+$: 279.1104, found: 279.1107.

*4.11.31. 1-(1H-benzo[d]imidazole-2-yl)-3-(3-fluorophenyl)urea (**10b**)*

White powder; yield 90%; m.p. 161–162 °C; ^{1}H NMR (400 MHz, DMSO-d_6) δ 11.32 (s, 1H), 9.63 (s, 1H), 7.65 (d, J = 12.10 Hz, 2H), 7.36 (m, 2H), 7.29 (m, 2H), 7.07 (m, 2H), 6.78 (m, 1H); ^{13}C NMR (100 MHz, DMSO-d_6) δ 164.1 (J = 240.32 Hz), 156.6, 150.5, 142.4, 142.3, 133.9, 130.7, 130.6, 121.7 (2C), 114.6 (J = 2.01 Hz), 112.7, 108.5 (J = 20.95 Hz), 105.3 (J = 26.97 Hz); HRMS (ESI)$^+$: calcd for $C_{14}H_{11}FN_4NaO$ [M + Na]$^+$: 293.0809, found: 293.0804.

*4.11.32. 1-(1H-benzo[d]imidazole-2-yl)-3-(4-(trifluoromethyl) phenyl)urea (**11b**)*

White powder; yield 91%; m.p. 197–200 °C; ^{1}H NMR (400 MHz, DMSO-d_6) δ 11.41 (s, 1H), 9.76 (s, 1H), 7.83 (d, J = 8.60 Hz, 2H), 7.63 (d, J = 8.60 Hz, 2H), 7.35 (m, 2H), 7.09 (m, 2H); ^{13}C NMR (100 MHz, DMSO-d_6) δ 157.3, 151.0, 144.4, 133.4, 126.4 (2C), 126.4, 123.7 (2C), 121.8, 118.4 (2C), 112.9, 112.5 (2C); HRMS (ESI)$^+$: calcd for $C_{15}H_{11}F_3N_4NaO$ [M + Na]$^+$: 343.0777, found: 343.0778.

*4.11.33. 1-(3-fluorophenyl)-3-(4-(trifluoromethyl)phenyl)urea (**12b**)*

White powder; yield 90%; m.p. 188–191 °C; ^{1}H NMR (400 MHz, DMSO-d_6) δ 9.16 (s, 1H), 9.03 (s, 1H), 7.65 (m, 4H), 7.49 (m, 1H), 7.32 (m, 1H), 7.15 (m, 1H), 6.81 (m, 1H); ^{13}C NMR (100 MHz, DMSO-d_6) δ 164.1(J = 241.07 Hz), 152.6, 143.7, 141.7, 141.6, 130.9, 130.8, 126.6 (J = 3.37 Hz), 126.5 (J = 3.65 Hz), 122.3 (J = 31.72 Hz), 118.5, 114.6 (J = 2.36 Hz), 108.9 (J = 21.41 Hz), 105.5 (J = 26.69 Hz); HRMS (ESI)$^+$: calcd for $C_{14}H_{10}F_4N_2NaO$ [M + Na]$^+$: 321.0621, found: 321.0629.

*4.11.34. 1-(3,5-bis(trifluoromethyl)benzyl)-3-(3-fluorophenyl)urea (**13b**)*

White powder; yield 93%; m.p. 185–188 °C, ^{1}H NMR (400 MHz, DMSO-d_6) δ 9.01 (s, 1H), 8.01 (s, 2H), 7.98 (s, 1H), 7.44 (m, 1H), 7.25 (q, J = 7.76 Hz, 1H), 7.08 (dd, J = 8.27 Hz, 0.95 Hz, 1H), 6.96 (t, J = 6.03 Hz, 1H), 6.71 (m, 1H), 4.48 (d, J = 5.94 Hz, 2H); ^{13}C NMR (100 MHz, DMSO-d_6) δ 161.7(J = 241.00 Hz), 155.6, 144.7, 142.7, 142.6, 130.5(J = 22.11 Hz), 130.4(J = 20.60 Hz), 128.4(J = 2.82 Hz), 125.2, 122.5, 120.9, 120.8, 114.0, 107.9(J = 20.69 Hz), 104.8(J = 25.86 Hz), 42.5; HRMS (ESI)$^+$: calcd for $C_{16}H_{11}F_7N_2NaO$ [M + Na]$^+$: 403.0652, found:403.0654.

*4.11.35. 1-(3,5-bis(trifluoromethyl)benzyl)-3-(4-(trifluoromethyl) phenyl)urea (**14b**)*

White powder; yield 92%; m.p. 166–167 °C; ^{1}H NMR (400 MHz, DMSO-d_6) δ 9.21 (s, 1H), 8.01 (s, 2H), 7.99 (s, 1H), 7.59 (m, 4H), 7.03 (t, J = 6.07 Hz, 1H), 4.50 (d, J = 5.98 Hz, 2H); ^{13}C NMR (100 MHz, DMSO-d_6) δ 155.5, 144.6, 144.5, 131.1, 130.8, 130.4, 130.1, 128.4(J = 2.65 Hz), 126.4(J = 3.71 Hz), 125.2, 123.7, 122.5, 121.9, 121.6, 120.9, 117.9, 42.6; HRMS (ESI)$^+$: calcd for $C_{17}H_{11}F_9N_2NaO$ [M + Na]$^+$: 453.0620, found: 453.0624.

*4.11.36. 4-(1-(2-(3-bromobenzoyl)hydrazono)ethyl)-N-(1H-pyrazol-3-yl)benzamide (**1c**)*

White powder; yield 73%; m.p. 198–199 °C; ^{1}H NMR (400 MHz, DMSO-d_6) δ 11.02 (s, 1H), 8.20 (d, J = 2.80 Hz, 1H), 7.98 (m, 6H), 7.80 (d, J = 7.34 Hz, 1H), 7.49 (t, J = 8.07 Hz, 1H), 6.04 (d, J = 2.96 Hz, 1H), 5.71 (s, 2H), 2.42 (s, 3H); ^{13}C NMR (100 MHz, DMSO-d_6) δ 162.3, 157.4, 152.4, 136.9, 134.5, 131.0, 130.8, 128.5, 128.0 (2C), 127.4 (2C), 126.5, 125.4, 122.1, 114.4, 66.4, 48.1, 14.9; HRMS (ESI)$^+$: calcd for $C_{19}H_{16}BrN_5NaO_2$ [M + Na]$^+$: 448.0379, found: 448.0387.

*4.11.37. 4-(1-(2-(3-fluoro-4-methylbenzoyl)hydrazono)ethyl)-N-(4-morpholinopyridin-2-yl)benzamide (**2c**)*

White powder; yield 65%; m.p. 234–236 °C; 1H NMR (400 MHz, DMSO-d_6) δ 10.95 (s, 1H), 10.56 (s, 1H), 8.22 (s, 1H), 8.00 (m, 6H), 7.78 (s, 1H), 7.33 (t, J = 7.78 Hz, 1H), 6.70 (q, J = 6.04 Hz, 2.28 Hz, 1H), 3.74 (m, 4H), 3.29 (m, 4H), 2.41 (s, 3H), 1.20 (s, 3H); 13C NMR (100 MHz, DMSO-d_6) δ 162.2, 161.9, 161.6, 160.0, 157.1, 153.6, 147.7, 141.5, 131.1, 132.8, 130.7, 128.9 (2C), 128.6 (2C), 126.8, 122.2, 113.5, 100.0, 95.1, 66.4 (2C), 52.3 (2C), 14.9, 10.8; HRMS (ESI)+: calcd for C26H26FN5NaO3 [M + Na]+: 498.1912, found: 498.1904.

*4.11.38. 3-bromo-N'-(1-(4-morpholinophenyl)ethylidene) benzohydrazide (**3c**)*

White powder; yield 79%; m.p. 209–210 °C; ^{1}H NMR (400 MHz, DMSO-d_6) δ 10.75 (s, 1H), 8.04 (s, 1H), 7.88 (t, J = 6.66 Hz, 1H), 7.75 (m, 3H), 7.48 (t, J = 8.14 Hz, 1H), 6.97 (d, J = 7.40 Hz, 2H), 3.74 (m, 4H), 3.19 (m, 4H), 2.29 (s, 3H); ^{13}C NMR (100 MHz, DMSO-d_6) δ 162.5 157.4, 152.4, 136.9, 134.5, 131.0, 130.8 (2C), 128.5, 127.4, 122.1, 114.4 (2C), 113.5, 66.4 (2C), 48.1 (2C), 14.9; HRMS (ESI)$^+$: calcd for $C_{19}H_{20}BrN_3NaO_2$ [M + Na]$^+$: 424.0631,found: 424.0639.

*4.11.39. 3-iodo-4-methyl-N'-(1-(4-morpholinophenyl)ethylidene) benzohydrazide (**5c**)*

White powder; yield 70%; m.p. 203–206 °C; ^{1}H NMR (400 MHz, DMSO-d_6) δ 10.70 (s, 1H), 8.30 (d, J = 1.14 Hz, 1H), 7.78 (m, 3H), 7.44 (d, J = 8.00 Hz, 1H), 6.96 (m, 2H), 3.74 (m, 4H), 3.19 (m, 4H), 2.44 (s, 3H), 2.29 (s, 3H); ^{13}C NMR (100 MHz, DMSO-d_6) δ 163.2, 152.3, 147.7, 144.9, 138.0, 130.1, 128.6 (2C), 128.2, 128.0, 126.3, 114.4 (2C), 98.3, 66.4 (2C), 48.1 (2C), 28.0, 14.9; HRMS (ESI)$^+$: calcd for $C_{20}H_{22}IN_3NaO_2$ [M + Na]$^+$: 486.0649, found: 486.0648.

*4.11.40. N-(1H-benzo[d]imidazole-2-yl)-4-(1-(2-(3-fluorobenzoyl) hydrazono)ethyl)benzamide (**6c**)*

White powder; yield 74%; m.p. 231–234 °C; ^{1}H NMR (400 MHz, DMSO-d_6) δ 12.22 (s, 2H), 10.85 (s, 1H), 8.09 (d, J = 8.71 Hz, 2H), 7.75 (d, J = 8.71 Hz, 2H), 7.48 (m, 3H), 7.15 (m, 2H), 6.67 (s, 2H), 2.06 (s, 3H); ^{13}C NMR (100 MHz, DMSO-d_6) δ 168.8, 168.3, 163.2, 149.2, 143.7, 141.0, 136.6 (2C), 135.1, 132.7, 130.4 (2C), 128.7 (2C), 124.9, 123.1, 121.9 (2C), 118.9 (2C), 115.2, 113.9, 11.7; HRMS (ESI)$^+$: calcd for $C_{23}H_{18}FN_5NaO_2$ [M + Na]$^+$: 438.1337, found: 438.1345.

*4.11.41. N-(1H-benzo[d]imidazole-2-yl)-4-(1-(2-(3-bromobenzoyl) hydrazono)ethyl)benzamide (**7c**)*

White powder; yield 63%; m.p. 247–250 °C; ^{1}H NMR (400 MHz, DMSO-d_6) δ 12.34 (s, 2H), 10.98 (s, 1H), 8.22 (m, 2H), 7.99 (m, 4H), 7.80 (t, J = 7.02 Hz, 1H), 7.48 (m, 3H), 7.15 (m, 2H), 2.43 (s, 3H); ^{13}C NMR (100 MHz, DMSO-d_6) δ 164.7, 163.2, 157.1, 153.6, 148.5, 141.5, 141.0, 136.5 (2C), 135.8, 134.9, 130.9 (2C), 128.5 (2C), 126.8, 123.4 (2C), 114.7 (2C), 105.9, 98.7, 16.7; HRMS (ESI)$^+$: calcd for $C_{23}H_{18}BrN_5NaO_2$ [M + Na]$^+$: 498.0536, found: 498.0542.

*4.11.42. 4-(1-(2-(3-bromobenzoyl)hydrazono)ethyl)-N-(4-morpholinopyridin-2-yl)benzamide (**8c**)*

White powder; yield 69%; m.p. 254–255 °C; ^{1}H NMR (400 MHz, DMSO-d_6) δ 10.98 (s, 1H), 10.55 (s, 1H), 7.92 (m, 9H), 7.48 (t, J = 7.26 Hz, 1H), 6.71 (q, J = 6.00 Hz, 1.96 Hz, 1H), 3.75 (m, 4H), 3.28 (m, 4H), 2.41 (s, 3H); ^{13}C NMR (100 MHz, DMSO-d_6) δ 164.2, 163.0, 160.1, 150.2, 149.7, 141.0, 140.9, 136.7 (2C), 136.4, 131.1, 127.9 (2C), 126.8, 122.0, 127.6, 126.5, 123.2, 100.0, 95.1, 66.5 (2C), 54.9 (2C), 15.2; HRMS (ESI)$^+$: calcd for $C_{25}H_{24}BrN_5NaO_3$ [M + Na]$^+$: 544.0955, found: 544.0949.

*4.11.43. 3-fluoro-N'-(1-(4-morpholinophenyl)ethylidene) benzohydrazide (**9c**)*

White powder; yield 75%; m.p. 210–212 °C; ^{1}H NMR (400 MHz, DMSO-d_6) δ 10.79 (s, 1H),7.97 (m, 2H),7.75 (m, 3H),7.48 (m, 1H), 6.98 (d, J = 8.07 Hz, 2H), 3.73 (m, 4H), 3.18 (m, 4H), 2.29 (s, 3H); ^{13}C NMR (100 MHz, DMSO-d_6) δ 167.6, 164.2, 152.3, 148.2, 141.0, 131.0, 127.9 (2C), 126.7, 120.0, 118.9, 114.5, 112.4 (2C), 66.5 (2C), 54.9 (2C), 15.2; HRMS (ESI)$^+$: calcd for $C_{19}H_{20}FN_3NaO_2$ [M + Na]$^+$: 364.1432, found: 364.1432.

*4.11.44. 4-(1-(2-(3-bromobenzoyl)hydrazono)ethyl)-N-morpholinobenzamide (**10c**)*

White powder; yield 77%; m.p. 203–205 °C; ^{1}H NMR (400 MHz, DMSO-d_6) δ 10.94 (s, 1H), 9.59 (s, 1H), 8.06 (s, 1H), 7.86 (m, 6H), 7.49 (t, J = 7.77 Hz, 1H), 3.67 (s, 4H), 2.90 (s, 4H), 2.39 (s, 3H); ^{13}C NMR (100 MHz, DMSO-d_6) δ 167.4, 164.2, 150.8, 148.9, 141.0, 136.7, 131.1, 129.5, 128.2, 127.9 (2C), 126.8 (2C), 122.0, 121.1, 66.5 (2C), 54.9 (2C), 15.2; HRMS (ESI)$^+$: calcd for $C_{20}H_{21}BrN_4NaO_3$ [M + Na]$^+$: 467.0689, found: 467.0692.

Declaration of competing interest

The authors declare that they have no known competing financial interests or personal relationships that could have appeared to influence the work reported in this paper.

Acknowledgement

National Science and Technology Major Project of the Ministry of Science and Technology of China (No. 2018ZX09735005); National Natural Science Foundation of China, Grant Numbers: 81922064, 81874290, and 81903502; China Postdoctoral Science Foundation, Grant Number: 2020M673268; The Fundamental Research Funds for the Central Universities, Grant Number: 2021SCU12102; Opening fund of State Key Laboratory of Esophageal Cancer Prevention and Treatment(Zhengzhou University), Grant Number: K2020-001.

Appendix A. Supplementary data

Supplementary data to this article can be found online at https://doi.org/10.1016/j.ejmech.2021.113424.

References

[1] N. Harbeck, M. Gnant, Breast cancer, Lancet 389 (2017) 1134–1350.
[2] C. Woolston, Breast cancer, Nature 527 (2015) S101.
[3] M. Kalimutho, K. Parsons, D. Mittal, J.A. Lopez, S. Srihari, K.K. Khanna, Targeted therapies for triple-negative breast cancer: combating a stubborn disease, Trends Pharmacol. Sci. 36 (2015) 822–846.
[4] R. Islam, K.W. Lam, Recent progress in small molecule agents for the targeted therapy of triple-negative breast cancer, Eur. J. Med. Chem. 1 (207) (2020), 112812.
[5] D. Elkhalifa, A.B. Siddique, M. Qusa, F.S. Cyprian, K. El Sayed, F. Alali, A.E. Al Moustafa, A. Khalil, Design, synthesis, and validation of novel nitrogen-based chalcone analogs against triple negative breast cancer, Eur. J. Med. Chem. 1 (187) (2020), 111954.
[6] D.F. Hayes, Further progress for patients with breast cancer, N. Engl. J. Med. 380 (7) (2019) 676–677.
[7] S. Kimbung, N. Loman, I. Hedenfalk, Clinical and molecular complexity of breast cancer metastases, Semin. Canc. Biol. 35 (2015) 85–95.
[8] A.G. Waks, E.P. Winer, Breast cancer treatment: a review, JAMA, J. Am. Med. Assoc. 321 (2019) 288–300.
[9] S. Lefort, C. Joffre, Y. Kieffer, A.M. Givel, B. Bourachot, G. Zago, I. Bieche, T. Dubois, D. Meseure, A. Vincent-Salomon, J. Camonis, F. Mechta-Grigoriou, Inhibition of autophagy as a new means of improving chemotherapy efficiency in high-LC3B triple-negative breast cancers, Autophagy 10 (12) (2014) 2122–2142.
[10] J.H. Park, K.P. Kim, J.J. Ko, K.S. Park, PI3K/Akt/mTOR activation by suppression of ELK3 mediates chemosensitivity of MDA-MB-231 cells to doxorubicin by inhibiting autophagy, Biochem Bioph Res Co 477 (2) (2016) 277–282.
[11] V. Karantza-Wadsworth, E. White, Role of autophagy in breast cancer, Autophagy 3 (6) (2007) 610–613.
[12] G. Yang, Y. Li, Y. Zhao, L. Ouyang, Y. Chen, B. Liu, J. Liu, Targeting Atg4B for cancer therapy: chemical mediators, Eur. J. Med. Chem. 1 (209) (2021), 112917.
[13] C.H. Chang, K. Bijian, D. Wernic, J. Su, S.D. da Silva, H. Yu, D. Qiu, M. Asslan, M.A. Alaoui-Jamali, A novel orally available seleno-purine molecule suppresses triple-negative breast cancer cell proliferation and progression to metastasis by inducing cytostatic autophagy, Autophagy 15 (8) (2019) 1376–1390.
[14] H. Xiang, J. Zhang, C. Lin, L. Zhang, B. Liu, L. Ouyang, Targeting autophagy-related protein kinases for potential therapeutic purpose, Acta Pharm. Sin. B 10 (4) (2020) 569–581.
[15] X. Chang, D. Sun, D. Shi, G. Wang, Y. Chen, K. Zhang, H. Tan, J. Liu, B. Liu, L. Ouyang, Design, synthesis, and biological evaluation of quinazolin-4(3H)-one derivatives co-targeting poly (ADP-ribose) polymerase-1 and bromodomain containing protein 4 for breast cancer therapy, Acta Pharm. Sin. B 11 (1) (2021) 156–180.

[16] M. Liao, J. Zhang, G. Wang, L. Wang, J. Liu, L. Ouyang, B. Liu, Small-molecule drug discovery in triple negative breast cancer: current situation and future directions, J. Med. Chem. 64 (5) (2021) 2382–2418.
[17] A. Kaur, S. Sharma, Mammalian target of rapamycin (mTOR) as a potential therapeutic target in various diseases, Inflammopharmacology 25 (3) (2017) 293–312.
[18] L. Asnaghi, P. Bruno, M. Priulla, A. Nicolin, mTOR: a protein kinase switching between life and death, Pharmacol. Res. 50 (6) (2004) 545–549.
[19] R. Loewith, E. Jacinto, S. Wullschleger, A. Lorberg, J.L. Crespo, D. Bonenfant, W. Oppliger, P. Jenoe, M.N. Hall, Two TOR complexes, only one of which is rapamycin sensitive, have distinct roles in cell growth control, Mol Cell 10 (3) (2002) 457–468.
[20] D.D. Sarbassov, S.M. Ali, D.H. Kim, D.A. Guertin, R.R. Latek, H. Erdjument-Bromage, P. Tempst, D.M. Sabatini, Rictor, a novel binding partner of mTOR, defines a rapamycin-insensitive and raptor-independent pathway that regulates the cytoskeleton, Curr. Biol. 14 (14) (2004) 1296–1302.
[21] K. Hara, Y. Maruki, X. Long, K. Yoshino, N. Oshiro, S. Hidayat, C. Tokunaga, J. Avruch, K. Yonezawa, Raptor, a binding partner of target of rapamycin (TOR), mediates TOR action, Cell 110 (2) (2002) 177–189.
[22] P.P. Hsu, S.A. Kang, J. Rameseder, Y. Zhang, K.A. Ottina, D. Lim, T.R. Peterson, Y. Choi, N.S. Gray, M.B. Yaffe, J.A. Marto, D.M. Sabatini, The mTOR-regulated phosphoproteome reveals a mechanism of mTORC1-mediated inhibition of growth factor signaling, Science 332 (6035) (2011) 1317–1322.
[23] T.T. Wu, Q.Q. Guo, Z.L. Chen, L.L. Wang, Y. Du, R. Chen, Y.H. Mao, S.G. Yang, J. Huang, J.T. Wang, L. Wang, L. Tang, J.Q. Zhang, Design, synthesis and bioevaluation of novel substituted triazines as potential dual PI3K/mTOR inhibitors, Eur. J. Med. Chem. 15 (204) (2020), 112637.
[24] T. Xu, D. Sun, Y. Chen, L. Ouyang, Targeting mTOR for fighting diseases: a revisited review of mTOR inhibitors, Eur. J. Med. Chem. 199 (2020), 112391.
[25] Y. Maejima, S. Kyoi, P. Zhai, T. Liu, H. Li, A. Ivessa, S. Sciarretta, D.P. Del Re, D.K. Zablocki, C.P. Hsu, D.S. Lim, M. Isobe, J. Sadoshima, Mst1 inhibits autophagy by promoting the interaction between Beclin1 and Bcl-2, Nat. Med. 19 (11) (2013) 1478–1488.
[26] R.A. Saxton, D.M. Sabatini, mTOR signaling in growth, metabolism, and disease, Cell 168 (6) (2017) 960–976.
[27] J. Li, S.G. Kim, J. Blenis, Rapamycin: one drug, many effects, Cell Metabol. 19 (2014) 373–379.
[28] F. Conciatori, L. Ciuffreda, C. Bazzichetto, I. Falcone, S. Pilotto, E. Bria, F. Cognetti, M. Milella, mTOR cross-talk in cancer and potential for combination therapy, Cancers 10 (1) (2018) 23.
[29] D. Benjamin, M. Colombi, C. Moroni, M.N. Hall, Rapamycin passes the torch: a new generation of mTOR inhibitors, Nat. Rev. Drug Discov. 10 (11) (2011) 868–880.
[30] T. Noda, Y. Ohsumi, Tor, a phosphatidylinositol kinase homologue, controls autophagy in yeast, J. Biol. Chem. 273 (7) (1998) 3963–3966.
[31] H. Yang, D.G. Rudge, J.D. Koos, B. Vaidialingam, H.J. Yang, N.P. Pavletich, mTOR kinase structure, mechanism and regulation, Nature 497 (7448) (2013) 217–223.
[32] M.L. Maddess, M.N. Tackett, H. Watanabe, P.E. Brennan, C.D. Spilling, J.S. Scott, D.P. Osborn, S.V. Ley, Total synthesis of rapamycin, Angew. Chem. Int. Ed. 46 (4) (2007) 591–597.
[33] E. López-Knowles, S.A. O'Toole, C.M. McNeil, E.K. Millar, M.R. Qiu, P. Crea, R.J. Daly, E.A. Musgrove, R.L. Sutherland, PI3K pathway activation in breast cancer is associated with the basal-like phenotype and cancer-specific mortality, Int. J. Canc. 126 (5) (2010) 1121–1131.
[34] G. Pérez-Tenorio, O. Stål, et al., Activation of AKT/PKB in breast cancer predicts a worse outcome among endocrine treated patients, Br. J. Canc. 86 (4) (2002) 540–545.
[35] Q. Fan, O. Aksoy, R.A. Wong, S. Ilkhanizadeh, C.J. Novotny, W.C. Gustafson, A.Y. Truong, G. Cayanan, E.F. Simonds, D. Haas-Kogan, J.J. Phillips, T. Nicolaides, M. Okaniwa, K.M. Shokat, W.A. Weiss, A kinase inhibitor targeted to mTORC1 drives regression in glioblastoma, Canc. Cell 31 (2017) 424–435.
[36] M. Yu, M. Zeng, Z. Pan, F. Wu, L. Guo, G. He, Discovery of novel akt1 inhibitor induces autophagy associated death in hepatocellular carcinoma cells, Eur. J. Med. Chem. 1 (189) (2020), 112076.
[37] T.F. Cloughesy, K. Yoshimoto, P. Nghiemphu, K. Brown, J. Dang, S. Zhu, T. Hsueh, Y. Chen, W. Wang, D. Youngkin, L. Liau, N. Martin, D. Becker, M. Bergsneider, A. Lai, R. Green, T. Oglesby, M. Koleto, J. Trent, S. Horvath, P.S. Mischel, I.K. Mellinghoff, C.L. Sawyers, Antitumor activity of rapamycin in a phase I trial for patients with recurrent PTEN- deficient glioblastoma, PLoS Med. 5 (1) (2008) e8.
[38] B. Apsel, J.A. Blair, B. Gonzalez, T.M. Nazif, M.E. Feldman, B. Aizenstein, R. Hoffman, R.L. Williams, K.M. Shokat, Z.A. Knight, Targeted polypharmacology: discovery of dual inhibitors of tyrosine and phosphoinositide kinases, Nat. Chem. Biol. 4 (11) (2008) 691–699.
[39] S.M. Maira, F. Stauffer, J. Brueggen, P. Furet, C. Schnell, C. Fritsch, S. Brachmann, P. Chène, A. De Pover, K. Schoemaker, D. Fabbro, D. Gabriel, M. Simonen, L. Murphy, P. Finan, W. Sellers, C. García-Echeverría, Identification and characterization of NVP-BEZ235, a new orally available dual phosphatidylinositol 3-kinase/mammalian target of rapamycin inhibitor with potent in vivo antitumor activity, Mol. Canc. Therapeut. 7 (7) (2008) 1851–1863.
[40] C.M. Chresta, B.R. Davies, I. Hickson, T. Harding, S. Cosulich, S.E. Critchlow, J.P. Vincent, R. Ellston, D. Jones, P. Sini, D. James, Z. Howard, P. Dudley, G. Hughes, L. Smith, S. Maguire, M. Hummersone, K. Malagu, K. Menear, R. Jenkins, M. Jacobsen, G.C. Smith, S. Guichard, M. Pass, AZD8055 is a potent, selective, and orally bioavailable ATP-competitive mammalian target of rapamycin kinase inhibitor with in vitro and in vivo antitumor activity, Canc. Res. 70 (1) (2010) 288–298.
[41] M.R. Janes, C. Vu, S. Mallya, M.P. Shieh, J.J. Limon, L.S. Li, K.A. Jessen, M.B. Martin, P. Ren, M.B. Lilly, L.S. Sender, Y. Liu, C. Rommel, D.A. Fruman, Efficacy of the investigational mTOR kinase inhibitor MLN0128/INK128 in models of B-cell acute lymphoblastic leukemia, Leukemia 27 (3) (2013) 586–594.
[42] Q.W. Fan, Z.A. Knight, D.D. Goldenberg, W. Yu, K.E. Mostov, D. Stokoe, K.M. Shokat, W.A. Weiss, A dual PI3 kinase/mTOR inhibitor reveals emergent efficacy in glioma, Canc. Cell 9 (5) (2006) 341–349.
[43] P. Tang, J. Zhang, J. Liu, C.M. Chiang, L. Ouyang, Targeting bromodomain and extraterminal proteins for drug discovery: from current progress to technological development, J. Med. Chem. 64 (5) (2021) 2419–2435.
[44] B. Ravikumar, C. Vacher, Z. Berger, J.E. Davies, S. Luo, L.G. Oroz, F. Scaravilli, D.F. Easton, R. Duden, C.J. O'Kane, D.C. Rubinsztein, Inhibition of mTOR induces autophagy and reduces toxicity of polyglutamine expansions in fly and mouse models of Huntington disease, Nat. Genet. 36 (6) (2004) 585–595.
[45] J.C. Choi, A. Muchir, W. Wu, S. Iwata, S. Homma, J.P. Morrow, H.J. Worman, Temsirolimus activates autophagy and ameliorates cardiomyopathy caused by lamin A/C gene mutation, Sci. Transl. Med. 4 (144) (2012) 102.
[46] B. Munafó Daniela, I. Colombo María, A novel assay to study autophagy: regulation of autophagosome vacuole size by amino acid deprivation, J. Cell Sci. 114 (2001) 3619–3629.
[47] J.F. Xue, Z.M. Shi, J. Zou, X.L. Li, Inhibition of PI3K/AKT/mTOR signaling pathway promotes autophagy of articular chondrocytes and attenuates inflammatory response in rats with osteoarthritis, Biomed. Pharmacother. 89 (2017) 1252–1261.
[48] L. Ouyang, L. Zhang, S. Zhang, D. Yao, Y. Zhao, G. Wang, L. Fu, P. Lei, B. Liu, Small-molecule activator of UNC-51-Like kinase 1 (ULK1) that induces cytoprotective autophagy for Parkinson's disease treatment, J. Med. Chem. 12; 61 (7) (2018) 2776–2792.
[49] S. Miller, A. Oleksy, O. Perisic, R.L. Williams, Finding a fitting shoe for Cinderella: searching for an autophagy inhibitor, Autophagy 6 (6) (2010) 805–807.
[50] Y. Zhen, R. Zhao, M. Wang, X. Jiang, F. Gao, L. Fu, L. Zhang, X.L. Zhou, Flubendazole elicits anti-cancer effects via targeting EVA1A-modulated autophagy and apoptosis in Triple-negative Breast Cancer, Theranostics 10 (18) (2020) 8080–8097.
[51] B. Cao, J. Li, X. Zhou, J. Juan, K. Han, Z. Zhang, Y. Kong, J. Wang, X. Mao, Clioquinol induces pro-death autophagy in leukemia and myeloma cells by disrupting the mTOR signaling pathway, Sci. Rep. 4 (2014) 5749.